Horizontal water vapor transport in the lower stratosphere from subtropics to high latitudes during boreal summer

F. Ploeger,[1] G. Günther,[1] P. Konopka,[1] S. Fueglistaler,[2] R. Müller,[1] C. Hoppe,[1] A. Kunz,[1,3] R. Spang,[1] J.-U. Grooß,[1] and M. Riese[1]

Received 22 March 2013; revised 26 June 2013; accepted 5 July 2013; published 31 July 2013.

[1] We compare global water vapor observations from Microwave Limb Sounder (MLS) and simulations with the Lagrangian chemical transport model CLaMS (Chemical Lagrangian Model of the Stratosphere) to investigate the pathways of water vapor into the lower stratosphere during Northern Hemisphere (NH) summer. We find good agreement between the simulation and observations, with an effect of the satellite averaging kernel especially at high latitudes. The Asian and American monsoons emerge as regions of particularly high water vapor mixing ratios in the lower stratosphere during boreal summer. In NH midlatitudes and high latitudes, a clear anticorrelation between water vapor and ozone daily tendencies reveals a large region influenced by frequent horizontal transport from low latitudes, extending up to about 450 K during summer and fall. Analysis of the zonal mean tracer continuity equation shows that close to the subtropics, this horizontal transport is mainly caused by the residual circulation. In contrast, at higher latitudes, poleward of about 50°N, eddy mixing dominates the horizontal water vapor transport. Model simulations with transport barriers confirm that almost the entire annual cycle of water vapor in NH midlatitudes above about 360 K, with maximum mixing ratios during summer and fall, is caused by horizontal transport from low latitudes. In the model, highest water vapor mixing ratios in this region are clearly linked to horizontal transport from the subtropics.

Citation: Ploeger, F., G. Günther, P. Konopka, S. Fueglistaler, R. Müller, C. Hoppe, A. Kunz, R. Spang, J.-U. Grooß, and M. Riese (2013), Horizontal water vapor transport in the lower stratosphere from subtropics to high latitudes during boreal summer, *J. Geophys. Res. Atmos.*, *118*, 8111–8127, doi:10.1002/jgrd.50636.

1. Introduction

[2] Water vapor is a major player in the Earth's radiation budget and critically affects stratospheric chemistry [e.g., *Forster and Shine*, 1999]. Changes in the distribution of water vapor, particularly in the upper troposphere and lower stratosphere (UTLS), strongly impact radiative forcing and surface temperatures [*Riese et al.*, 2012] and are of key importance for understanding climate change [*Solomon et al.*, 2010]. Therefore, an improved understanding of those processes governing the distribution of water vapor in the UTLS is a prerequisite for reliable climate predictions.

[3] Water vapor enters the stratosphere across the cold tropical tropopause in the tropical tropopause layer (TTL) [e.g., *Fueglistaler et al.*, 2009a], where freeze-drying causes strong dehydration from large tropospheric to very low stratospheric mixing ratios. As a consequence, the seasonality of tropical tropopause temperatures is imprinted on tropical stratospheric water vapor mixing ratios ascending with the Brewer-Dobson circulation, creating the famous water vapor "tape recorder" signal [*Mote et al.*, 1996]. To first order, water vapor mixing ratios in the tropical lower stratosphere are determined by the Lagrangian saturation history of air, enabling simplified prediction models based on large-scale advection and temperatures [e.g., *Fueglistaler et al.*, 2005; *Schiller et al.*, 2009]. Microphysical processes concerning nucleation and supersaturation, subgrid-scale temperature fluctuations as caused by gravity waves, and convection are important for understanding the details of dehydration [e.g., *Jensen and Pfister*, 2004].

[4] In the extratropical UTLS [e.g., *Gettelman et al.*, 2011], air is a mixture of aged air masses, which have been transported with the stratospheric (Brewer-Dobson) circulation through the deep stratosphere, and of young air masses, which have been transported isentropically from low to high latitudes or convectively upward from the troposphere [e.g., *Holton et al.*, 1995]. The aged air masses transported into the extratropical lower stratosphere from above have been subject to methane oxidation. Methane oxidation represents an important source for water vapor in the

[1]Institute of Energy and Climate Research, Stratosphere (IEK-7), Forschungszentrum Jülich, Jülich, Germany.
[2]Department of Geosciences, Princeton University, Princeton, New Jersey, USA.
[3]Institute for Atmospheric and Climate Science, ETH Zuerich, Zuerich, Switzerland.

Corresponding author: F. Ploeger, Institute of Energy and Climate Research, Stratosphere (IE-7), Forschungszentrum Jülich, 52 425 Jülich, Germany. (f.ploeger@fz-juelich.de)

©2013. American Geophysical Union. All Rights Reserved.
2169-897X/13/10.1002/jgrd.50636

middle stratosphere [e.g., *Jones and Pyle*, 1984; *Rohs et al.*, 2006], and the downwelling air has a moistening effect. The strength of isentropic transport between low and high latitudes decreases with height in the lower stratosphere and becomes very weak at altitudes of the tropical pipe [e.g., *Plumb*, 2002]. This decrease is not sharp but gradual, with satellite and in situ observations indicating a large region in the extratropical lower stratosphere influenced by young air from low latitudes [e.g., *Ray et al.*, 1999; *Bönisch et al.*, 2008]. During summer, these low latitude air masses have relatively high water vapor mixing ratios and act to moisten the extratropics [e.g., *Rosenlof et al.*, 1997; *Pan et al.*, 1997]. However, based on observations alone, it appears difficult to quantify the contributions of horizontal isentropic transport and of downward transport of aged air on moistening the extratropical lower stratosphere.

[5] Horizontal poleward transport in the lower stratosphere is related both to advection by the residual circulation and to isentropic eddy mixing [*Plumb*, 2002]. Breaking Rossby-waves both drive the Brewer-Dobson circulation and provide a mechanism for stirring the air [*McIntyre and Palmer*, 1983] and for quasi-horizontal isentropic transport between tropics and extratropics [e.g., *Randel et al.*, 1993; *Riese et al.*, 2002]. Related intrusions of low latitude air may reach deep into midlatitudes and high latitudes [e.g., *Pan et al.*, 2009]. The seasonality of horizontal transport depends on the seasonality in the strength of subtropical mixing barriers, which are known to be weakest in the summer hemisphere [*Haynes and Shuckburgh*, 2000].

[6] A related mechanism for moistening the lowermost part of the extratropical UTLS during summer has been proposed by *Dethof et al.* [1999], involving midlatitude synoptic disturbances interacting with the Asian monsoon anticyclone. During these interactions, moist air filaments are drawn out of the anticyclone and transported into NH extratropics. Within the lowermost part of the stratosphere, in the extratropical tropopause layer [*Fischer et al.*, 2000; *Hoor et al.*, 2002] extending within about 30 K distance of the extratropical local tropopause [*Hoor et al.*, 2004; *Hegglin et al.*, 2009], additional processes may play a role, involving baroclinic instability and convection [e.g., *Gettelman et al.*, 2011].

[7] The subtropics are critical regions for understanding the transport of water vapor within the UTLS, as the highest UTLS water vapor mixing ratios occur in the subtropical Asian and American monsoons during boreal summer [e.g., *Bian et al.*, 2012; *Schwartz et al.*, 2013]. Air masses, transported upward from the boundary layer, are partially confined within the anticyclonic monsoon circulations and are subsequently lifted further up [*Park et al.*, 2006]. Along the eastern flanks, the monsoon anticyclones transport air masses equatorward, affecting trace gas budgets in the tropics [*Konopka et al.*, 2009; *Ploeger et al.*, 2012]. Along the western flanks, the flow is directed poleward. Recent studies have shown evidence for the Asian monsoon to act as an efficient transport pathway into the lower stratosphere [*Gettelman et al.*, 2004; *Randel et al.*, 2010]. However, transport of the high monsoon water vapor mixing ratios to the tropical and extratropical lower stratosphere, in particular a potential amplification of the tropical water vapor tape recorder, remains a matter of debate [e.g., *Bannister et al.*, 2004; *Wright et al.*, 2011].

[8] In this paper, we analyze the transport of water vapor into the extratropical lower stratosphere in the altitude region above the subtropical jet, based on global satellite observations and model simulations. The good agreement between our model simulation and observations allows a closer look at many details and quantification of certain processes. The aim of this paper is to: (i) characterize the lower stratosphere region where water vapor is influenced by frequent horizontal transport from low latitudes, (ii) analyze the impact of this horizontal transport on the seasonal cycle and on the high summer and fall mixing ratios of water vapor in the NH lower stratosphere, and (iii) investigate the processes involved.

[9] The data and model simulations are described in section 2. In section 3, we compare observed and simulated water vapor in the lower stratosphere, with a particular focus on seasonal variations, and show that the simulation agrees well with observations. This agreement is the basis for the following analysis of horizontal water vapor transport between subtropics, extratropics, and tropics in section 4, using three different approaches (tracer-tracer correlations, transport barriers, and tracer continuity equation), which provide complementary information. We conclude with a detailed discussion in section 5.

2. Data and Method

2.1. MLS Satellite Observations

[10] We compare water vapor observations in the lower stratosphere from the Microwave Limb Sounder (MLS) instrument onboard the Aura satellite (version 3.3 data) and simulations using the Chemical Lagrangian Model of the Stratosphere (CLaMS) for the period 2005–2010. Detailed information on MLS water vapor and the retrieval procedure can be found in *Read et al.* [2007] and *Lambert et al.* [2007].

[11] In the UTLS, the region of interest for our study, the vertical resolution of MLS water vapor is around 3 km. We find that the MLS averaging kernel induces some artifacts, in particular at high latitudes, as discussed in detail in section 3.2. We interpolated all profiles to potential temperature (θ) levels and carried out most analyses on surfaces of constant potential temperature, adequate to the near isentropic nature of horizontal transport between tropics and extratropics. MLS scans about 3500 profiles per day and provides a high-frequency sampling of the global atmosphere. This high-frequency sampling enables to investigate daily zonal mean time series of MLS observations (see section 4.1).

2.2. Lagrangian Transport Model CLaMS

[12] The CLaMS model [e.g., *McKenna et al.*, 2002a, 2002b; *Konopka et al.*, 2007] is a Lagrangian chemistry transport model, based on three-dimensional forward trajectories describing the motion of air parcels, denoted CLaMS air parcels in the following. Irreversible small-scale mixing between CLaMS air parcels is parameterized in the model and induced by deformations in the large-scale atmospheric flow. Consequently, in regions of large flow deformations, large mixing occurs.

[13] The model transport is calculated in the hybrid vertical coordinate system proposed by *Mahowald et al.* [2002].

The hybrid vertical coordinate transforms from an orography following σ-coordinate at the lower boundary into potential temperature θ above $\sigma = 0.3$ (with $\sigma = p/p_s$, pressure p and surface pressure p_s, this transition occurs at about 300 hPa above most areas of the globe). Consequently, advective transport in the model is purely diabatic above the tropopause and even throughout the entire TTL, with vertical velocity $\dot{\theta}$ deduced from the diabatic heating rate. Recent comparisons between diabatic and kinematic transport calculations emphasized the benefits of diabatic transport for simulating stratospheric water vapor [e.g., *Schoeberl and Dessler*, 2011; *Ploeger et al.*, 2011]. The Lagrangian diabatic model CLaMS has demonstrated its particular advantages in simulating steep tracer gradients and small-scale filamentary structures [e.g., *Konopka et al.*, 2004].

[14] We carried out a multiyear CLaMS simulation covering the period from 1 October 2001 to 31 December 2010, based on wind and temperature data from European Centre for Medium-range Weather Forecasts (ECMWF) ERA-Interim reanalysis. The total diabatic heating rate for the calculation of the cross-isentropic vertical velocity $\dot{\theta}$ is taken from ERA-Interim forecast data, as described by *Ploeger et al.* [2010]. The heating rates include the contributions of all-sky radiation, latent heat release, and diffusive and turbulent heat transport [*Fueglistaler et al.*, 2009b]. The model domain extends from the Earth's surface to the stratopause. Further details concerning the specific CLaMS model setup will be described in Konopka et al. (in preparation).

[15] The calculation of water vapor mixing ratios in the model CLaMS is based on a simplified dehydration scheme, similar to that applied by *von Hobe et al.* [2011]. The lower boundary for the water vapor mixing ratio calculation is located at approximately 500 hPa. Below, mixing ratios are set to the ERA-Interim water vapor field every day, and a vanishing ice water content is assumed. If saturation occurs along a CLaMS air parcel trajectory, the water vapor amount in excess of the saturation mixing ratio is instantaneously transformed to the ice phase. The freeze-drying time step of the temperature trajectory is 6 h. An empirically determined ice particle density based on in situ observations [*Krämer et al.*, 2009] is used to calculate a mean ice particle radius from the CLaMS air parcel ice water content, as well as the corresponding terminal settling velocity. The corresponding sedimentation length is compared to a characteristic length (300 m, the approximate vertical model resolution around the tropical tropopause), and a respective fraction of ice is removed. The effects of the finite settling velocity are critically discussed in section 5. If the parcel is undersaturated and ice exists, ice is instantaneously evaporated to maintain saturation. Methane oxidation is included as an additional source for water vapor in the middle and upper stratosphere, with the amounts of hydroxyl, oxygen, and chlorine radicals taken from a model climatology [*Pommrich et al.*, 2011]. Sensitivities of simulated water vapor to the specific dehydration scheme are discussed in section 5.5.

2.3. Satellite-Model Comparison With Averaging Kernel

[16] For an improved comparison of model data to satellite observations, the effects of the MLS averaging kernel have been taken into account. Therefore, we first mapped the model data onto the MLS measurement locations, using back trajectories, before applying the weighting due to the satellite averaging kernels. The MLS averaging kernels can be found in *Read et al.* [2007] and *Livesey et al.* [2011], where further details about the averaging kernels are discussed. The averaging kernels were applied to the model water vapor profiles using pressure as the vertical coordinate and the logarithm of the water vapor mixing ratio. Finally, the data was mapped to potential temperature surfaces for each day and the monthly climatologies were created.

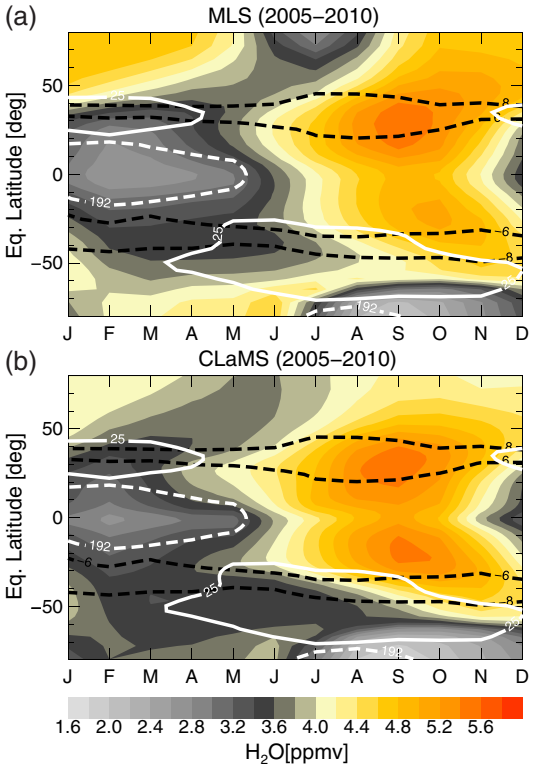

Figure 1. Latitude-time variations of water vapor at 390 K from (a) MLS and (b) CLaMS, from a 2005–2010 climatology. Temperature (192 K) as white dashed, zonal winds (25 m/s) as white solid, and PV (±6, ±8 PVU (potential vorticity unit)) as black dashed contours.

[17] In the following, we explicitly indicate results based on model data with additionally accounting for the averaging kernel. In section 3.2, we explicitly discuss characteristics of MLS lower stratosphere water vapor observations related to the satellite averaging kernel.

3. Simulated Versus Observed Lower Stratosphere Water Vapor

3.1. Seasonal Variations of Water Vapor

[18] The seasonal variations of water vapor in the lower stratosphere at 390 K are shown in the equivalent latitude versus time presentation of Figure 1 (as monthly 2005–2010 climatology). We use potential vorticity (PV)-based equivalent latitude as meridional coordinate [*Nash et al.*, 1996] to eliminate the effects of reversible transport [e.g., *Olsen et al.*, 2010]. The good agreement between the seasonal structures in the MLS satellite observations and the CLaMS water

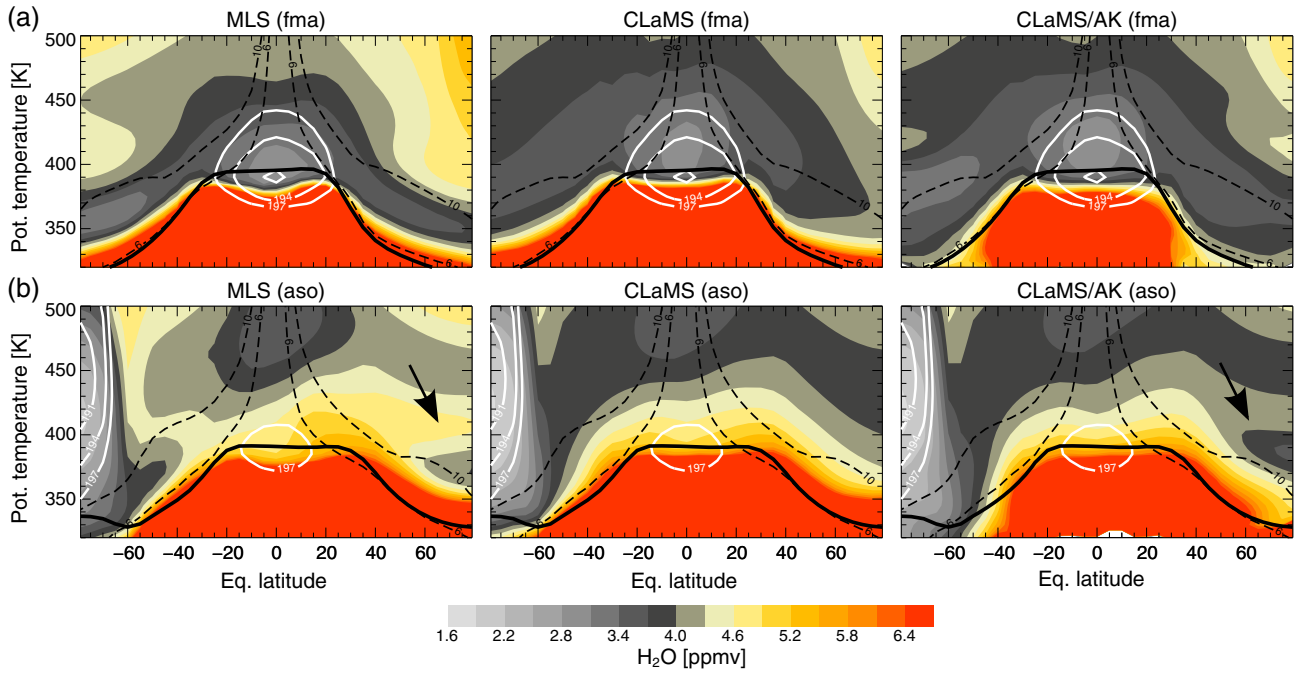

Figure 2. Zonal mean water vapor from (left) MLS, (middle) CLaMS, and (right) CLaMS with accounting for the MLS averaging kernel for (a) February–April "fma" and (b) August–October "aso" 2005–2010. White lines are the temperature, black dashed lines are the PV, and the black solid line is the tropopause. The zonal mean is based on the calculated tropopause (see text). Arrows indicate regions influenced by the MLS averaging kernel.

vapor simulation provides confidence in the reliability of the simulated water vapor field.

[19] Tropical water vapor shows a clear annual cycle with highest mixing ratios during boreal summer and fall and lowest mixing ratios during winter, linked to the annual cycle of tropical tropopause temperatures (white dashed contours). The water vapor mixing ratios in the subtropics and midlatitudes of both hemispheres show similar annual cycles, with maxima during boreal fall. Highest mixing ratios appear in the subtropics around August-September, particularly on the NH. Figure 1 suggests propagation of these high subtropical water vapor mixing ratios to higher latitudes and, to a lesser extent, also equatorward, favored by the weak latitudinal PV gradient in the subtropics during summer and fall [compare *Randel et al.*, 2001]. On the NH, the moist signal reaches higher latitudes compared to the SH, where extremely cold temperatures within the Antarctic polar vortex efficiently dehydrate the air between July and October. Note that in boreal summer, during the warm phase of TTL temperatures, water vapor mixing ratios in the inner tropics are lower than over the subtropics indicating that not all air masses pass the tropical temperature minimum [see also *Wright et al.*, 2011]. We will thoroughly analyze this horizontal transport in section 4.

[20] Additional information on water vapor transport into the extratropical lower stratosphere is provided by zonal mean MLS observations in Figure 2 (left column). The zonal average is calculated using the distance to the thermal tropopause (in θ), based on the temperature lapse rate [*World Meteorological Organization*, 1957], as vertical coordinate [compare *Birner et al.*, 2002], to precisely present the structures in the UTLS water vapor distribution. The tropopause-based vertical coordinate ensures that in the zonal averaging dynamically equivalent situations are compared (e.g., stratospheric air inside a tropopause fold is compared to stratospheric air). For better illustration, the mean tropopause potential temperature has been added to the vertical coordinate before plotting in Figure 2.

[21] Clearly, the NH midlatitude and high latitude lower stratosphere below about 430 K shows highest water vapor mixing ratios during summer and fall (August–October "aso," in Figure 2b) compared to winter and spring (February–April "fma," in Figure 2a). The moistening of the NH lower stratosphere occurs gradually from boreal summer to fall. For both seasons (February–April and August–October), there is reliable agreement between MLS observations (left column) and the simulation (middle column), although the moistening effect of downwelling aged air during hemispheric winter appears to be weaker in the model than observed by MLS. Further differences concerning layered structures in the observation at high latitudes are likely related to the satellite averaging kernel and will be discussed in section 3.2. Note that observations and simulation both show enhanced water vapor mixing ratios in the subtropics around the tropopause, in particular on the summer hemisphere.

[22] In addition to horizontal transport from low latitudes, downwelling of moist air from the middle stratosphere may contribute to the moistening of the lower stratosphere. During boreal winter and spring (Figure 2a), strong downwelling in the NH extratropics, related to the Brewer-Dobson circulation, transports moist air masses downward. These air masses are moister than the air below, due to methane oxidation in the middle stratosphere. During boreal summer and

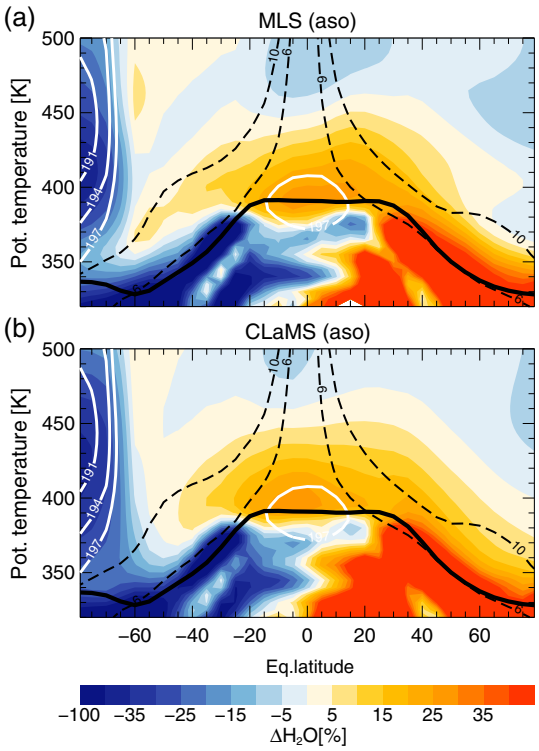

Figure 3. Zonal mean annual cycle for water vapor (as relative anomaly) from (a) MLS and (b) CLaMS for August–October (aso) 2005–2010. Temperature contours as white lines, PV as black dashed lines, the tropopause as thick black lines.

fall (Figure 2b), the season of maximum water vapor mixing ratios on the NH, strongest subsidence occurs on the SH.

[23] The effects of horizontal transport and downwelling can be further separated by considering the annual anomaly of zonal mean water vapor (relative to the annual mean in percent) in Figure 3, for August–October ("aso"). The agreement between the model simulation and the observations is even better than for the mixing ratios in Figure 2. Within a large region, including the tropical, NH, and parts of the SH lower stratosphere, the annual water vapor maximum occurs during boreal summer and fall. Above about 430 K, the NH annual water vapor cycle is in its negative phase (minimum) and likely linked to downwelling of aged moist air, which is weaker in summer than in winter. Below about 430 K, the annual cycle has the opposite phase (maximum in summer), and the coherent seasonal variation of the tropical and extratropical lower stratosphere suggests that the annual cycle in that region is likely caused by horizontal transport from low latitudes. The effects of this horizontal transport on midlatitude and high latitude water vapor will be further investigated in section 4.

[24] The global water vapor distribution at 390 K during boreal summer (July–September) from MLS in Figure 4a shows highest water vapor mixing ratios in the NH subtropical jet region. In particular, the Asian and American monsoons emerge as regions with very high mixing ratios. Furthermore, the entire subtropical jet shows slightly enhanced water vapor mixing ratios. The overall agreement between MLS observations and the model simulation (Figure 4b) is good. But the observations indicate slightly moister air masses above America compared to Asia, whereas the simulation shows moistest air in the Asian monsoon region, an aspect further discussed in *James et al.* [2008]. Hence, comparison of observations and simulation shows no coherent picture concerning the relative impact of the two monsoons. Remarkably, the model simulation shows frequent transport of moist air from the Asian monsoon along the jet to the American monsoon region. Hence, even in the MLS observations in Figure 4a, a certain amount

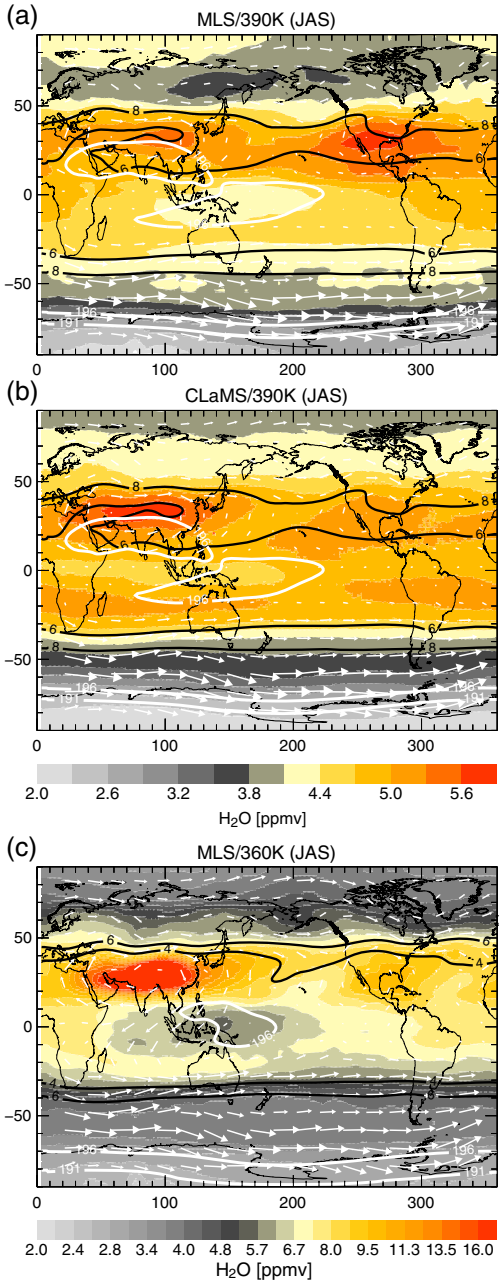

Figure 4. Water vapor distribution for July–September (JAS) 2005–2010, from (a) MLS and (b) CLaMS at 390 K, and for (c) MLS at 360 K. The 196 K temperature contour as white line, PV contours (±4,6,8 PVU) as black lines, and horizontal winds as white arrows (meridional wind v scaled by factor 6).

of the moist air observed above Central America at 390 K might originate in the Asian monsoon at lower levels.

[25] At potential temperature surfaces of 360 K and below, both MLS observations (Figure 4c) and the simulation (not shown) show highest water vapor mixing ratios, by far, in the Asian monsoon region. This indicates that the air transported upward in the monsoon circulation remains confined within the anticyclone [*Park et al.*, 2006]. The discrepancy in the moisture at 390 K within the Asian and American monsoons between the model and MLS observations cannot be attributed to the MLS averaging kernel and requires further attention (see also our discussion in section 5.4). Here, we focus on horizontal transport of moist air from the entire subtropics, irrespective of the monsoon origin of this moisture.

3.2. Effects of the MLS Averaging Kernel

[26] The zonal mean MLS observations in the left column of Figure 2 show an oscillation pattern at high latitudes, which is not reproduced in the model simulation (middle column). For an improved comparison to MLS observations, the model data was smoothed with the satellite averaging kernel (Figure 2, right column), as described in section 2.3. The effect of the averaging kernel turns out to be small in the tropics but larger in the extratropics. In particular, at high latitudes, accounting for the averaging kernel causes oscillations in the water vapor simulation. A layer of enhanced mixing ratios appears slightly above 400 K and a layer of decreased mixing ratios directly below (see arrows in Figure 2), compared to the "pure" model simulation without accounting for the averaging kernel.

[27] Particularly, during August–October, observation and simulation both show a layer of enhanced water vapor mixing ratios extending from NH subtropics to high latitudes at about 400–430 K (arrows). This layer is related to the broad averaging kernel at these altitudes, which involves large mixing ratios from the lowermost stratosphere directly above the tropopause. The dry layer below is related to negative values in the averaging kernel at levels around the tropopause. Consequently, the oscillation pattern in MLS water vapor in the lower stratosphere at high latitudes is likely an artifact of the MLS averaging kernel, and not representing atmospheric structure.

4. Horizontal Transport to Midlatitudes and High Latitudes

4.1. Low Latitude Air Intrusions

[28] The horizontal water vapor distributions at 400 K in Figure 5 show a typical transport event in the vicinity of the Asian monsoon. On 12 August 2005, a filament of enhanced water vapor is drawn out of the monsoon on the eastern flank of the anticyclone at about 110°E longitude. Daily water vapor maps show that immediately before that date highest water vapor mixing ratios were confined within the anticyclone (not shown). Already a few days later, in 17 August, the filament extends to NH polar regions and is subsequently mixed with the NH midlatitude background air. Note that the process described is similar to the mechanism for moistening the lowermost stratosphere proposed by *Dethof et al.* [1999], but occurring at much higher altitudes.

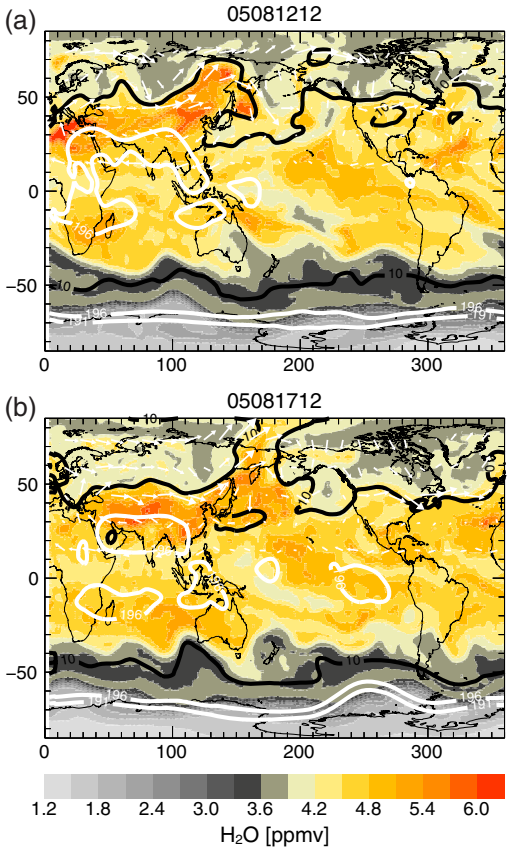

Figure 5. Water vapor distribution at 400 K for (a) 12 and (b) 17 August 2005, from the CLaMS simulation. The black line is the 10 PVU, the white line is the 196 K temperature contour, and the white arrows are the horizontal wind on the NH (v scaled by factor 3).

[29] Water vapor mixing ratios within the filament are more than 1 ppmv higher than the midlatitude background. The filamentary structure is reflected in the distribution of potential vorticity (PV, black contours in Figure 5). The high water vapor mixing ratios within the filament coincide with low PV values, indicating an intrusion of low latitude air. Latitude/θ sections (not shown) reveal that the intrusion covers a large area in the vertical, extending throughout the NH lower stratosphere to about 440 K.

[30] Remnants of similar intrusion events can be found on 12 August 2005 in NH midlatitudes at about 60°E and 200°E (Figure 5). These filamentary structures become largely eroded in 17 August. Daily global distributions of CLaMS water vapor show that these filamentation events occur rather often, in particular during boreal summer and fall on the NH (not shown). Furthermore, filamentation occurs not only in the vicinity of the monsoon anticyclones, but alongside the subtropical jets. The filaments typically exist for a couple of days (about 1 week in the example of Figure 5).

[31] The filamentary nature of water vapor transport to midlatitudes is reflected in the day-to-day variability of water vapor mixing ratios. Figure 6a shows the zonal mean water vapor mixing ratio at about 65°N and 390 K for the period 2005–2010, as observed by MLS. In addition to the annual cycle, there is a large day-to-day variability,

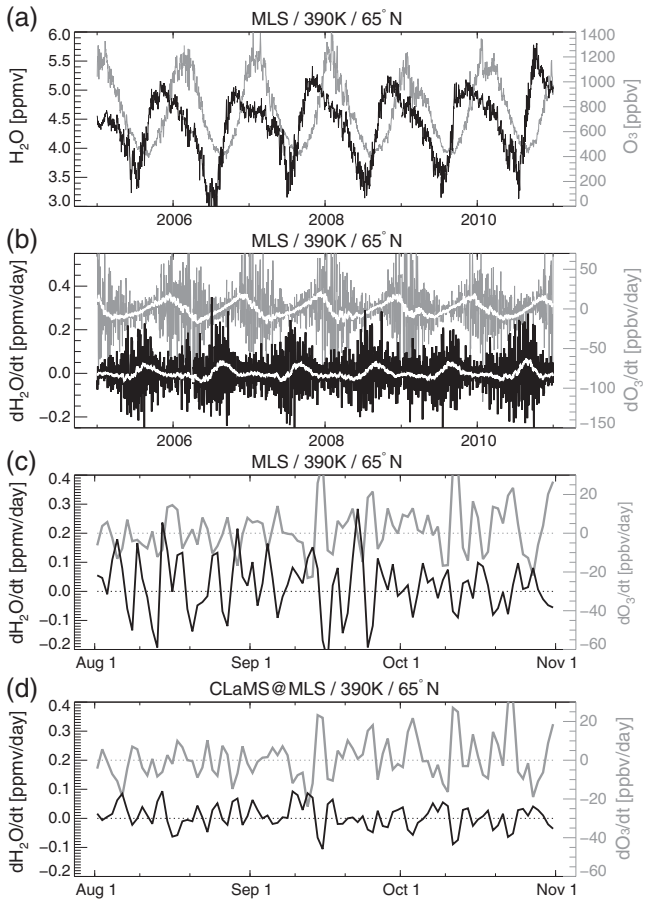

Figure 6. (a) Time series of MLS observed zonal mean water vapor (black) and ozone (gray) at 390 K at about 65° latitude for the period 2005–2010 (note that the black and gray *y* axes for water vapor and ozone, respectively). (b) Same as Figure 6a, but for daily tendencies of water vapor and ozone (white are time series smoothed with a 30 day running mean and multiplied with factor 2 for better visibility). (c) Same as Figure 6b, but for the period 1 August 2006 to 31 October 2006. (d) Same as Figure 6c, but for the CLaMS simulation with accounting for the MLS averaging kernel.

much larger than at tropical latitudes (not shown). This pronounced variability becomes even clearer in the time series of the daily water vapor mixing ratio tendency $\partial_t[H_2O]$ in Figure 6b (in ppmv/day). Large day-to-day changes up to 0.3 ppmv/day (about 10% of the zonal mean water vapor mixing ratio) are frequently observable in the time series.

[32] There is evidence for a pronounced seasonality in the water vapor day-to-day variability, with largest variability during boreal summer to fall and weakest variability during winter and spring. Hence, NH midlatitude and high latitude water vapor mixing ratios are not smoothly increasing during summer and fall, but change very abruptly from day to day, caused by the transport of moist filaments of low latitude air. The average water vapor tendency (white line, showing the daily tendency smoothed with a 30 day boxcar average) shows that the high-frequency daily tendency includes a net seasonal increase during summer and fall and a decrease during spring, as expected from the water vapor time series in Figure 6a.

[33] In contrast, the ozone day-to-day variability shows a reversed seasonality with largest variability during boreal winter to spring (gray line in Figure 6b). The seasonality in the variability of CLaMS simulated water vapor and ozone (not shown) is in good agreement with the variability in the MLS observations.

[34] To emphasize the connection between the water vapor and the ozone day-to-day variability, Figure 6c shows the zonal mean water vapor and ozone tendencies for the shorter period August–October 2006. The time series of water vapor and ozone tendencies show a clear anticorrelation, with positive water vapor changes accompanied by negative ozone changes. Our focus here is on altitudes high above the extratropical tropopause where direct convective upward transport is unlikely (moreover, in the model, we ensured that the impact of midlatitude convection is negligible, see sections 4.2 and 5.3). Therefore, this anticorrelation between water vapor and ozone tendencies shows that the high variability is caused by horizontal transport. In particular, intrusions from low latitudes during summer and fall are characterized by high water vapor and low ozone mixing ratios, and cause positive water vapor and negative ozone tendencies, simultaneously. Note that ozone could be replaced with PV in the above argumentation (not shown).

[35] Although the exact values of the zonal mean tendencies differ between MLS and CLaMS (Figure 6c/6d), CLaMS water vapor generally shows positive tendencies where the MLS water vapor tendency is positive and negative tendencies where the MLS water vapor tendency is negative. Hence, the model seems to simulate realistic intrusion processes, with a low latitude air intrusion occurring in the model whenever one occurs in the satellite data, albeit the simulated intrusions may occur at different longitudes and with different strengths.

[36] In the following, we will use the observed anticorrelation between water vapor and ozone time series to characterize the region in the midlatitude and high latitude lower stratosphere which is affected by horizontal transport from low latitudes. At each latitude and potential temperature location, we calculate the linear correlation coefficient for the correlation between the water vapor and ozone tendency time series. In the particular case of 65° latitude and 390 K for August–October 2006 (Figure 6c/6d), this results in correlation coefficients of –0.42 for MLS and –0.87 for CLaMS data, respectively, expressing a strong anticorrelation. As most filaments are reversible, returning to low latitudes without mixing with the midlatitude background air, we will use equivalent latitude as meridional coordinate for the following analysis. This reduces the effects of reversible transport [e.g., *Olsen et al.*, 2010].

[37] The equivalent latitude/θ-dependence of the linear correlation coefficient for the correlation between water vapor and ozone tendency time series for climatological August–October (2005–2010) from MLS and CLaMS is shown in Figure 7a. Negative correlation (blue) marks regions where high water vapor coincide with low ozone mixing ratios. Positive correlation (yellow) corresponds to regions where high water vapor and high ozone mixing ratios coincide. The sign of the correlation allows to distinguish between horizontal transport from low latitudes and vertical transport of aged air from above into the extratropical lower stratosphere. This distinction is possible because

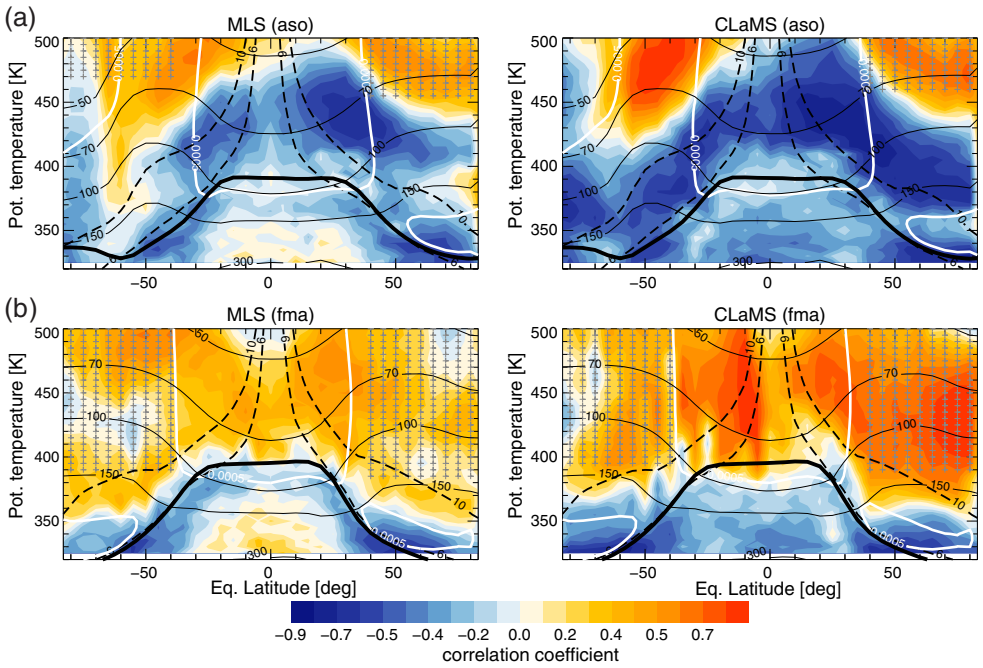

Figure 7. (a) Correlation coefficients (color coded) for the correlation between zonal mean (left) MLS and (right) CLaMS water vapor and ozone tendency time series at each latitude/potential temperature location, for August–October "aso" (2005–2010). Black lines show pressure, gray lines PV (±6, ±10 PVU), white lines Brunt-Vaisala frequency N^2 (5×10^{-4}s^{-2}). Altitudes with mean water vapor at midlatitudes higher than at low latitudes are hatched with crosses (see text). The zonal mean is based on the calculated tropopause (see text). (b) Same as Figure 7a, but for February–April 2005–2010.

low latitude air masses show high water vapor and low ozone, whereas subsiding aged air from the midstratosphere has both high ozone and high water vapor mixing ratios. Further analysis using transport barriers in the CLaMS model confirms that at altitudes above the subtropical jet core ($\theta > 360$ K), vertical upward transport, which would also cause a negative correlation, has a vanishing impact on the mean midlatitude lower stratosphere water vapor budget (see section 4.2). Further limitations to the relation between horizontal transport and a negative correlation coefficient will be discussed below.

[38] Overall, there is good agreement between the pattern of correlation coefficients from MLS and the CLaMS model for both August–October (Figure 7a) and February–April (Figure 7b). Hence, the simulated and observed water vapor and ozone variabilities agree well, providing confidence in the reliability of horizontal transport in the model simulation. The layer of positive correlation in NH high latitudes below 400 K is related to the MLS averaging kernel (compare section 3.2) and is only reproduced in the model simulation with accounting for the averaging kernel (not shown). Because of these averaging kernel effects, we consider the "pure" model simulation, in the following.

[39] During August–October, the negative correlations in Figure 7a (right) indicate a large region in the extratropical lower stratosphere, extending up to about 430–450 K, where water vapor is strongly influenced by horizontal transport from low latitudes. Above, the correlation becomes positive and water vapor is largely influenced by downwelling of aged air (which has been subject to methane oxidation). Note that also at these levels, the daily variability is dominated by horizontal transport, transporting aged air, which has been downwelling at high latitudes, equatorward. Furthermore, the anticorrelation is stronger and extends over a larger region on the NH than on the SH. This indicates a stronger impact of horizontal water vapor transport on the NH than on the SH. The influence of subsiding air on lower stratospheric water vapor, on the other hand, is strongest on the winter hemisphere.

[40] The "pure" model simulation shows a larger region of even stronger anticorrelations in NH midlatitudes and high latitudes during summer/fall, compared to MLS observations. On the one hand, the stronger anticorrelation in the model could indicate model deficiencies, but it could also be related to the models' ability to better resolve small-scale filaments, compared to the satellite observations. Global observations of higher resolution, as could be obtained from new limb imaging techniques [e.g., *Riese et al.*, 2005], may clarify this point and potentially provide a clearer distinction between vertically and horizontally controlled regions.

[41] During February–April (Figure 7b), the region of anticorrelation extends only up to about 350 K, indicating a much smaller region influenced by horizontal transport compared to summer/fall. However, during winter, the tropical water vapor tape recorder is in its dry phase, and mixing ratios around the tropical tropopause are lower than midlatitude values. Consequently, the unique relation between horizontal transport and a negative correlation coefficient breaks down. Areas in Figure 7 hatched with crosses indicate regions where the mean tropical water vapor mixing ratio on the respective hemisphere (0°–40°N/S equivalent latitude) is lower than the extratropical mean mixing ratio

(40°–80° equivalent latitude) and where horizontal transport therefore would cause a positive correlation. During boreal winter/spring, this reversal in the latitudinal water vapor gradient occurs around 390 K. During summer/fall, the water vapor gradient reversal occurs at about 460 K. The change from a negative to a positive correlation occurs below the level of gradient reversal during both winter and summer. Hence, for both seasons, a weakening of the impact of horizontal transport at levels where the correlation coefficient changes sign appears plausible, but we cannot exclude influence of horizontal transport above the level of gradient reversal (see also section 5.2).

[42] Further, we note a layer around 350 K just above the extratropical tropopause with lower correlation coefficients than above and below (Figure 7a, right). This minimum indicates weakened horizontal transport across the subtropical transport barrier at heights of the subtropical jet, and approximately coincides with the local maximum in static stability (measured in terms of the Brunt-Vaisala frequency N^2) of the tropopause inversion layer [*Birner*, 2006]. This aspect may be of importance to the radiative formation of the summer inversion layer [e.g., *Randel et al.*, 2007; *Kunz et al.*, 2009] and requires further attention.

4.2. Annual Water Vapor Cycle

[43] To quantify the impact of horizontal transport from the subtropical regions on mean water vapor mixing ratios in midlatitudes and in the tropics, we carry out simulations with transport barriers along latitude circles inserted into the CLaMS model, blocking transport between low and high latitudes. Two different simulations are carried out for 2005–2006, with transport barriers extending vertically from 320 to 520 K potential temperature and centered at latitudes 15°N/S (denoted CLaMS-Lat15) and at 35°N/S (CLaMS-Lat35), respectively. Because CLaMS is a Lagrangian, trajectory-based, transport model such barriers can be realized without changing the dynamics. The transport barriers have a width of 10° and are impermeable to both advective transport and parameterized small-scale mixing.

[44] Figure 8 shows the annual cycle of the water vapor mixing ratio in NH midlatitudes and in the tropics at 390 K (monthly climatology for 2005–2006) from the CLaMS reference simulation (Figure 8a) and from the two simulations with transport barriers (Figure 8b/8c). In NH midlatitudes, the reference simulation shows a clear annual cycle with maximum during summer and fall and minimum during winter and spring (Figure 8a). The summer/fall maximum disappears completely with transport barriers at 35° (CLaMS-Lat35 in Figure 8b). Consequently, the water vapor maximum in NH midlatitudes is related to horizontal transport from equatorward 40°N. With barriers at 15° (CLaMS-Lat15 in Figure 8c), the summer/fall maximum is very similar to the reference case without a barrier, but the winter/spring minimum appears much weaker. Therefore, the summer/fall maximum of NH water vapor is caused by horizontal transport of moist air from the subtropics between 20°N and 40°N, whereas the winter/spring minimum is caused by horizontal transport of very dry air from the tropics equatorward 20°N.

[45] For tropical water vapor, barriers at 35°N/S have a negligible effect (Figure 8b). With barriers at 15°N/S

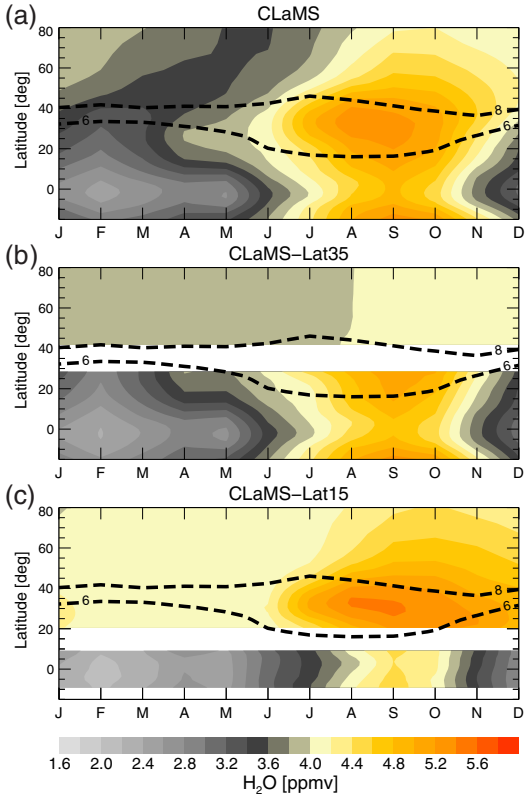

Figure 8. (a) Latitude-time variations of water vapor at 390 K from CLaMS for 2005–2006 (±6, ±8 PVU as black dashed contours). (b) Same as Figure 8a, but for the simulation with barriers centered at 35°N/S (CLaMS-Lat35). (c) Same as Figure 8b, but with barriers centered at 15°N/S (CLaMS-Lat15).

(Figure 8c), the mean tropical water vapor mixing ratios become dryer by about 0.5–1 ppmv. Hence, horizontal transport from midlatitudes has only a very small effect, whereas horizontal transport from the subtropics has a moistening effect on the deep tropics. The subtropical contribution to tropical water vapor shows only a very weak seasonality, and therefore, we find only a weak effect of subtropical processes, like monsoons, on amplifying the tropical seasonality, in agreement with *Wright et al.* [2011].

[46] Figure 9 presents the vertical dependence of the annual anomaly of water vapor in NH midlatitudes (relative to the annual mean), calculated from a monthly climatology for 2005–2006 for the reference simulation (Figure 9a) and for the two sensitivity simulations CLaMS-Lat35 (Figure 9b) and CLaMS-Lat15 (Figure 9c). The reference simulation (Figure 9a) shows a clear annual cycle with maximum during summer and fall. In the lowermost stratosphere (around 350 K), the water vapor maximum appears during July, about 3 months earlier than at about 400 K. The vertical structure in the anomaly resembles the tropical tape recorder.

[47] With barriers at 35° (CLaMS-Lat35), the NH water vapor annual cycle disappears completely above about 360 K (Figure 9b). Moreover, with barriers at 35°, the phase propagation of the water vapor maximum is downward, with the maximum at 460 K around June and at 400 K around

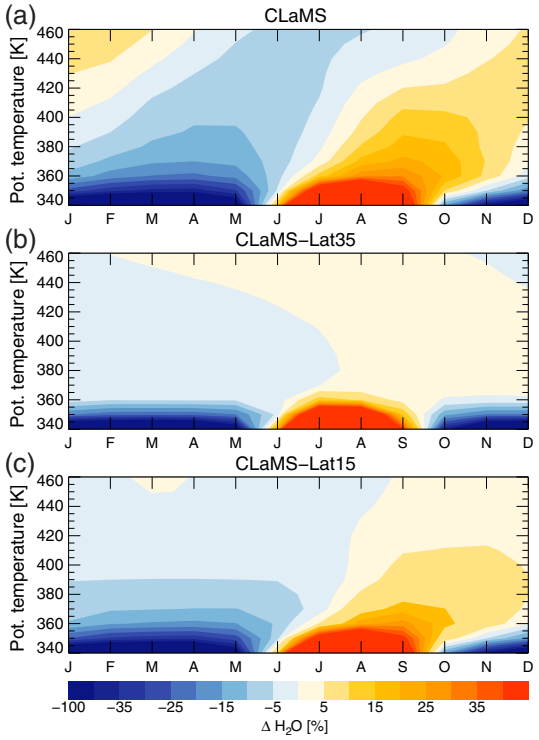

Figure 9. (a) Annual anomaly of water vapor (relative to annual mean) in NH midlatitudes (50°N–70°N equivalent latitude) from the reference CLaMS simulation for 2005–2006. (b) Same as Figure 9a, but for the sensitivity simulation with barriers centered at 35°N/S (CLaMS-Lat35). (c) Same as Figure 9b, but with barriers centered at 15°N/S (CLaMS-Lat15).

November, and is likely related to downwelling of moist air from above. Consequently, the upward phase propagation of the midlatitude water vapor maximum in the reference simulation, and likewise in observations (not shown), is related to horizontal transport from low latitudes. With barriers at 15° (CLaMS-Lat15 in Figure 9c), the annual cycle is similar to the reference case, although slightly attenuated. As we found already for the 390 K potential temperature level (Figure 8), horizontal transport of dry air from the tropics causes the winter/spring minimum and therefore increases the annual cycle of midlatitude water vapor.

[48] Further details about the effects of the transport barriers are presented in Figure 10, showing the probability density function (pdf) for water vapor mixing ratio in NH midlatitudes between 370 and 420 K during summer and fall from the model simulations and MLS observations. The reference simulation (gray shading) shows a long tail of the pdf, with high water vapor mixing ratios exceeding 6 ppmv. The distribution from MLS observations (light gray) is similar to the model result. Only at very low mixing ratios below about 3 ppmv MLS shows a higher frequency of occurrence. However, these differences have no consequence for our further conclusions, as we concentrate on the very high mixing ratios within the tail of the pdf (see section 5.3). Transport barriers at 15°N (CLaMS-Lat15) show an almost vanishing effect on the pdf (thin black line). In the simulation with transport barriers at 35°N (CLaMS-Lat35), however, the tail of high mixing ratios disappears completely (black shading). Hence, in the model, the high water vapor mixing ratios in NH midlatitudes are clearly caused by horizontal transport from the subtropics. These findings will be further discussed in section 5.3.

[49] Note that for all our above findings, a vertical barrier at about 340 K poleward 40° latitude, blocking upward transport from the extratropical troposphere directly into the extratropical stratosphere, has a vanishing effect on the midlatitude and high latitude mean water vapor mixing ratio above about 370 K (not shown). Hence, in the model, the NH water vapor budget at altitudes above the subtropical jet is unaffected by direct vertical transport from the extratropical troposphere.

[50] Although more sophisticated methods exist to determine the boundary between tropics and extratropics [e.g., *Kunz et al.*, 2011], in the above figures, we chose a fixed equivalent latitude value for simplicity. Note that we repeated the analysis for different (equivalent) latitude values (30°, 40°, and 50°) and confirmed that our conclusions are independent of the explicit choice of boundary.

4.3. Advective Transport Versus Eddy Mixing

[51] A natural way to separate the effects of advective transport by the residual circulation and eddy mixing

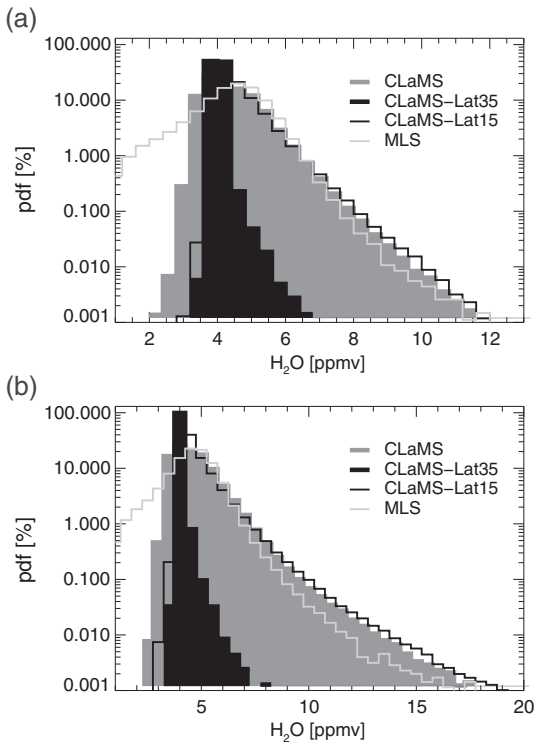

Figure 10. (a) Probability density function (pdf) of water vapor mixing ratios in NH midlatitudes (40°N–70°N latitude, with equivalent latitude ≥40°N, 370–420 K) for July–October (2005–2006 climatology). CLaMS reference simulation as gray shading, sensitivity simulation, with barriers at 35°N (15°N) as black shading (black line), MLS observations for 2005–2006 period as light gray line. (b) Same as Figure 10a, but without applying the equivalent latitude criterion to separate (sub-)tropical from midlatitude air.

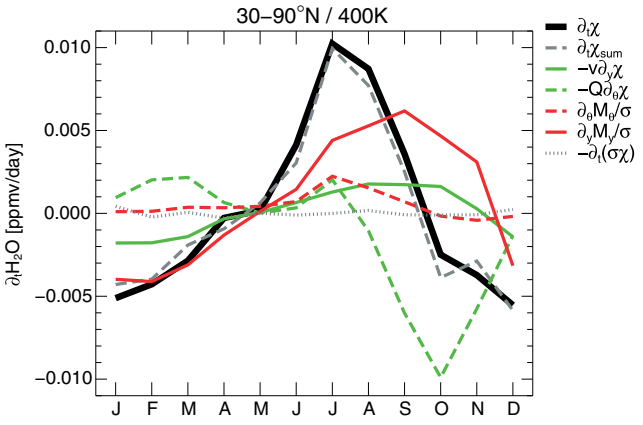

Figure 11. Seasonal variations of tendency terms in the isentropic zonal mean continuity equation for water vapor mixing ratio, at 400 K averaged over the NH extratropics between 30°N and 90°N (monthly means of 2005–2010 climatology; in the legend $y = a\varphi$).

on horizontal transport into the extratropical lower stratosphere is to analyze the Transformed Eulerian Mean (TEM) tracer continuity equation [e.g., *Andrews et al.*, 1987]. We apply a similar approach, but based on the isentropic zonal mean continuity equation for trace gas mixing ratio χ [e.g., *Andrews et al.*, 1987, equation (9.4.21)]

$$\partial_t \overline{\chi} = -\frac{\overline{v}^*}{a}\partial_\varphi \overline{\chi} - \overline{Q}^* \partial_\theta \overline{\chi} - \frac{1}{\overline{\sigma}}\partial_t(\overline{\sigma'\chi'}) + \frac{1}{\overline{\sigma}}\nabla \cdot M. \qquad (1)$$

Here the overbar represents the zonal mean (taken along surfaces of constant potential temperature), primed quantities (below) departures from the zonal mean, $\sigma = -g^{-1}\partial_\theta p$ is the density in isentropic coordinates, a is the Earth's radius, g is the acceleration due to gravity, φ is the latitude, p is the pressure, and ∇ is the horizontal gradient operator. The diabatic heating term $Q = \dot{\theta}$ equals the vertical cross-isentropic velocity. For a field X, the mass-weighted field is defined by $\overline{X}^* = (\overline{\sigma X})/\overline{\sigma}$.

[52] The first two terms on the right-hand side of equation (1) contain the effects of horizontal and vertical advective transport on the water vapor tendency. This advective transport is caused by the diabatic residual circulation $(\overline{v}^*, \overline{Q}^*)$. The last term on the right-hand side of equation (1) contains the eddy transport effects, within the divergence of the eddy flux vector M. The horizontal and vertical components of M are given by

$$M_\varphi = -\overline{(\sigma v)'\chi'}, \quad M_\theta = -\overline{(\sigma Q)'\chi'}. \qquad (2)$$

A similar analysis, but based on the TEM tracer continuity equation and concerning ozone and CO in the tropics, has been recently published by *Abalos et al.* [2012]. Because our focus is on horizontal transport which is nearly isentropic (moreover, CLaMS is an isentropic transport model), we apply an analysis based on isentropic levels. In the following, the notation advective transport refers to the first two terms on the right-hand side of equation (1), while eddy transport refers to the last term (divergence of M).

[53] Figure 11 shows the seasonal variation of the various contributions to the water vapor tendency in the NH extratropical lower stratosphere at 400 K and averaged between 30°N and 90°N, according to equation (1). The small difference between the left-hand (black) and right-hand (gray

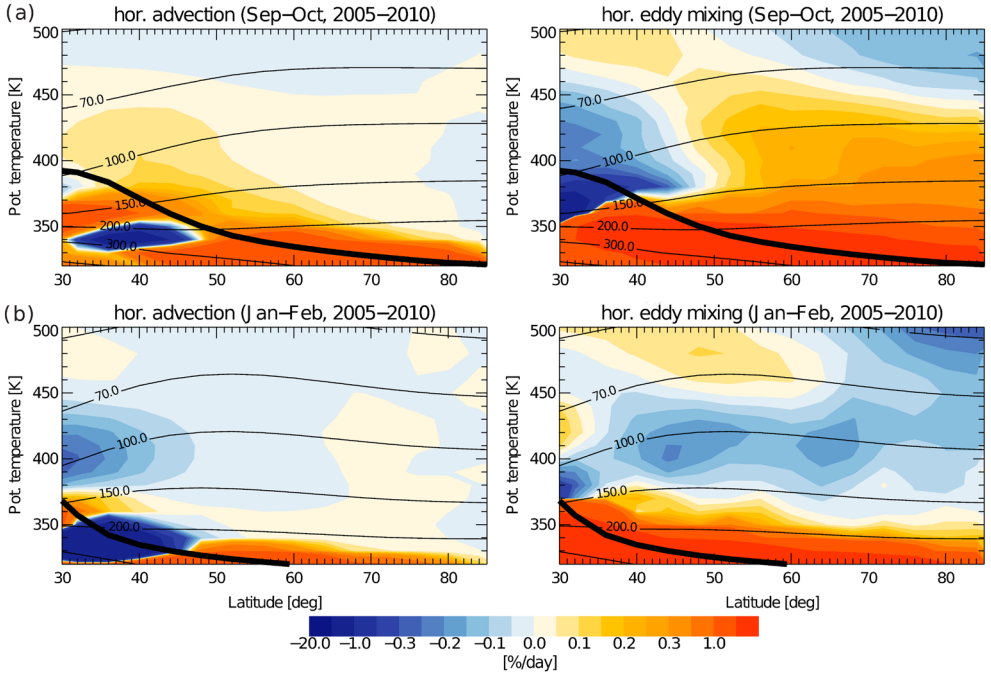

Figure 12. (a) (left) Horizontal advective tendency and (right) horizontal eddy tendency from isentropic zonal mean continuity equation for water vapor mixing ratio during September-October (2005–2010), as percentage of zonal mean water vapor mixing ratio (i.e., $-(\frac{\overline{v}^*}{a}\partial_\varphi\overline{\chi})/\overline{\chi}$ and $\frac{1}{\overline{\sigma}a\cos\varphi}\partial_\varphi(M_\varphi\cos\varphi)/\overline{\chi}$). Thermal tropopause as thick black, isobars as thin black lines. (b) Same as Figure 12a, but for January-February.

dashed) side of equation (1) shows that the calculated budget is almost closed and that the budget analysis is a reliable approach. In other regions of the atmosphere, e.g., around the tropical tropopause, water vapor mixing ratios are strongly affected by freeze-drying, chemistry, or small-scale mixing processes, and the zonal mean budget approach would require additional terms.

[54] The net water vapor tendency $\partial_t \overline{\chi}$ (black, left-hand side of equation (1)) shows a clear annual cycle, with positive values indicating increasing water vapor mixing ratios during boreal summer and fall (June–October) and negative values during winter and spring. The two dominant terms throughout the course of the year are vertical advection (green dashed) and horizontal eddy transport (red solid). Both terms show opposite annual cycles, with maximum/minimum for horizontal eddy/vertical advective transport during boreal summer and fall. The seasonality of the net tendency (black) approximately follows the horizontal eddy transport contribution. Clearly, the largest positive contribution to the net tendency during summer and fall, by far, is related to horizontal eddy mixing. The effect of meridional advection by the residual circulation appears to be much weaker (green solid). Downward advection of aged air (green dashed) causes an attenuation of the net seasonality and is most important for decreasing the water vapor tendency during boreal fall and winter. Note that the $\partial_t(\overline{\sigma'\chi'})$-term in equation (1) can be neglected in the budget (black dotted line).

[55] Figure 12 shows the full latitude/height-dependence of the horizontal advective and eddy tendencies during boreal fall (September–October) and winter and spring (January–February). During summer and fall, both eddy and advective horizontal transport cause a water vapor increase throughout most of the NH lower stratosphere below about 450 K. Close to the subtropics, this water vapor increase is related to horizontal advection by the diabatic residual circulation. At higher latitudes, larger than about 50°, horizontal eddy transport causes the increase of water vapor mixing ratios during NH summer and fall below about 450 K. During winter, both advective and eddy horizontal transport cause increasing water vapor mixing ratios in NH midlatitudes and high latitudes below about 360 K only. Above, the effect of horizontal transport decreases the midlatitude and high latitude mixing ratio, as air around the tropical tropopause is extremely dry during winter.

4.4. Asian Monsoon Pathway Into Lower Stratosphere

[56] Horizontal water vapor maps indicate that the Asian and American monsoon circulations act as moisture sources for the NH subtropical and extratropical lower stratosphere during boreal summer and fall (e.g., Figure 4 in section 4). We include two additional inert tracers in the CLaMS model simulation tagging the origin of air [*Günther et al.*, 2008], to further investigate the impact of convective upward transport within the monsoons on the lower stratosphere.

[57] The first tracer is an Asian monsoon tracer and is initialized on each day in the lowest model layer (orography following) in the Asian monsoon region (60°E–110°E, 5°N–40°N) with unity mixing ratio. The second tracer is an American monsoon tracer (245°E–295°E, 5°N–40°N). Above the initialization layer both tracers evolve freely subject to model transport. Hence, the tracer amounts at an arbitrary location represent the fractions of air, which have been transported from the boundary layer via the Asian and American monsoons during summer. The following results are not sensitive to slight variations of the geographical initialization regions.

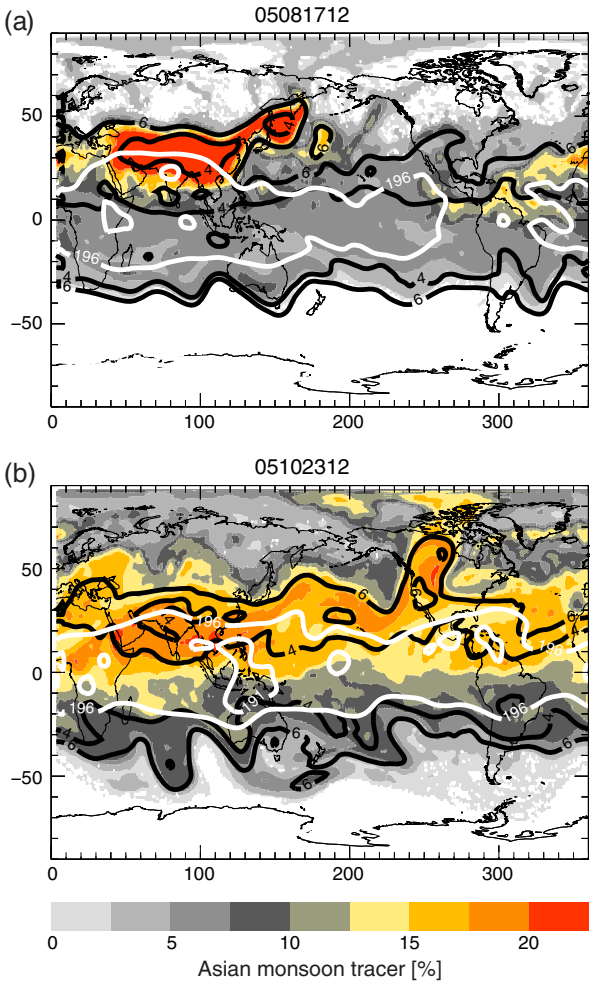

Figure 13. Map of Asian monsoon model tracer percentage at 380 K for (a) 17 August and (b) 23 October 2005. Black lines PV contours (±4, ±6 PVU), white lines temperature (191, 196 K).

[58] The horizontal distribution at 380 K in Figure 13a shows that during the active monsoon season, the Asian monsoon tracer is largely confined within the Asian monsoon anticyclone. This confinement is, however, not perfect, and air masses may leave the anticyclonic circulation into the NH subtropical jet. At the end of summer, when the monsoon anticyclone breaks up, the confined air is released into the jet, as shown in the Asian monsoon tracer distribution for 23 October 2005 (Figure 13b). The monsoon air is subsequently transported from the NH subtropical jet to high latitudes within horizontal filaments, as illustrated by the event around 250° longitude. Small-scale mixing processes irreversibly mix the monsoon air into the NH background. Consequently, the NH midlatitude and high latitude lower stratosphere is gradually filled with monsoon air during summer and fall.

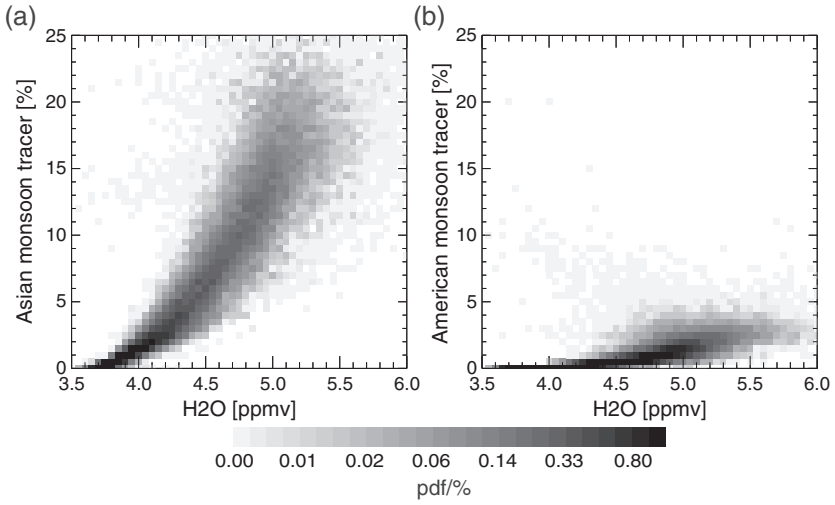

Figure 14. Correlation between CLaMS simulated water vapor and the (a) Asian and (b) American monsoon tracers in NH midlatitudes (50°N–90°N, 380–420 K), for the period 20–31 October 2005.

[59] Figure 14 shows the correlation between NH lower stratospheric water vapor (in the region 50°N–90°N and 380–420 K) and the Asian (Figure 14a) and American (Figure 14b) monsoon tracer mixing ratios. A strong and compact correlation emerges between NH water vapor and the Asian monsoon tracer. Hence, larger fractions of Asian monsoon air imply higher water vapor mixing ratios. Likewise, water vapor mixing ratios are positively correlated with the American monsoon tracer. We will further discuss these findings in section 5.4. Note that a substantial amount of Asian monsoon air is also transported into the tropics (see Figure 13) and potentially enters the ascending branch of the Brewer-Dobson circulation. Only very small amounts of monsoon air are transported farther to SH midlatitudes across the strong SH subtropical jet. Transport of moisture from the Asian monsoon into the tropics will be limited by the low temperatures above the Indian Ocean and West Pacific.

5. Discussion

[60] We analyzed the transport of water vapor into the lower stratosphere, based on MLS satellite observations and on simulations with the Chemical Lagrangian Model of the Stratosphere (CLaMS). We found good agreement between MLS observations and the model simulation with taking the MLS averaging kernel into account. The MLS averaging kernel causes oscillations in the zonal mean water vapor distribution at high latitudes (section 3.2). Particular emphasis was placed on horizontal transport from the subtropics to high latitudes at altitudes above the subtropical jet. Our results show evidence for a significant impact of this horizontal transport on water vapor in the extratropical lower stratosphere, particularly during boreal summer and fall.

5.1. Subtropical Pathway Into the Lower Stratosphere

[61] We further characterized the pathway of water vapor into the lower stratosphere during boreal summer and fall, based on both model and satellite data. Upward transport of water vapor within the Asian and American monsoon circulations appears to be the main moisture source for the upper troposphere and lower stratosphere during boreal summer, with highest water vapor mixing ratios confined within the monsoon anticyclones. But moist air masses also leave the monsoon circulation and moisten the region of the NH subtropical jet. Subsequently, the moist subtropical air is horizontally transported poleward moistening the NH midlatitudes and high latitudes during summer and fall.

[62] The moistening related to this "subtropical pathway" is significant, causing the whole summer/fall maximum of water vapor mixing ratios in the NH extratropical lower stratosphere above about 360 K, as confirmed by additional simulations with transport barriers in the model. We expect this transport pathway to be important also for other trace gas species, like sulfur-containing species of volcanic or anthropogenic origin.

[63] Advective horizontal transport by the residual circulation causes the summertime increase of water vapor close to the subtropics. Eddy horizontal transport causes the increase of water vapor mixing ratios in midlatitudes and high latitudes poleward of about 50°N. These findings support the concept that the Brewer-Dobson circulation includes a shallow branch which transports air masses from the tropical UTLS poleward [e.g., *Plumb*, 2002; *Birner and Bönisch*, 2011]. As potential changes in the circulation pattern have been shown to be critical for trends in the UTLS trace gas composition [e.g., *Bönisch et al.*, 2011; *Ray et al.*, 2010], a detailed understanding of related transport processes is important. Our results show a significant impact of residual circulation transport (advective transport) within this shallow Brewer-Dobson circulation branch only equatorward of about 50°. At higher latitudes, transport related to eddy mixing dominates the water vapor variability. Inspection of daily water vapor maps from the CLaMS simulation and of the day-to-day variability in observed and simulated zonal mean water vapor and ozone time series corroborates the finding that horizontal transport to high latitudes occurs abruptly within deep intrusions of low latitude air, which are likely related to Rossby-wave breaking. Poleward transport

of low ozone air within these intrusions has been recently analyzed by *Pan et al.* [2009].

[64] In the deep tropics, transport from the subtropics causes a constant moistening effect throughout the year, but no amplification of the water vapor seasonality. Hence, the tropical tape recorder signal appears largely unaffected by horizontal transport from the subtropics.

5.2. Seasonality of Horizontal Influence

[65] During boreal summer and fall, the anticorrelation between zonal mean time series of water vapor and ozone tendencies shows a large midlatitude and high latitude region with water vapor variability related to horizontal transport, extending up to about 450 K (see section 4.1). The H_2O-O_3 tendency anticorrelation maximizes around 370–430 K, indicating a maximum effect of horizontal transport from low latitudes in that region. This result agrees well with *Berthet et al.* [2007], who found a "ventilated layer," strongly influenced by rapid transport from the boundary layer, in the same altitude region during the same season. During winter, the effect of horizontal transport on midlatitude water vapor changes around 380 K, from moistening below to drying above (see Figure 12). The correlation approach indicates weak horizontal transport above 350 K (positive correlation), at altitudes of the jet core. Above about 380 K, the positive correlation allows no distinction between effects of horizontal transport and transport of aged stratospheric air from above, because of the dry phase of the water vapor tape recorder in the tropics (see section 4.1). However, a larger region in the lower stratosphere influenced by horizontal transport from low latitudes during boreal summer/fall compared to winter/spring, would be in good agreement with recently published papers. The age of air analysis of *Bönisch et al.* [2008] showed that the NH lower stratospheric air is youngest during summer and fall. Moreover, investigations of the O_3-N_2O correlation by *Hegglin and Shepherd* [2007] indicate a "flushing" of this region with young tropical air up to about 430 K from summer to fall.

[66] Horizontal water vapor transport to high latitudes is likely related to breaking Rossby-waves. In a recent paper, *Homeyer and Bowman* [2012] showed that poleward transport related to Rossby-wave breaking reverses seasonality at altitudes above 420 K. Above 420 K, transport maximizes during hemispheric winter (in agreement with *Waugh* [1996] and *Postel and Hitchman* [1999]), and below transport maximizes during hemispheric summer and fall. In the NH lower stratosphere, the maximum Rossby-wave breaking during summer/fall coincides with the highest water vapor mixing ratios in the (sub-)tropics, resulting in strong poleward transport of moist air (see Figure 1). In the SH lower stratosphere, the maximum Rossby-wave breaking in winter/spring coincides with lowest water vapor mixing ratios in the (sub-)tropics, resulting in strong poleward transport of dry air. In agreement with the seasonality of Rossby-wave breaking, the poleward transport of moist air in summer/fall appears stronger in the NH, whereas the poleward transport of dry air is stronger in the SH (see Figure 1). The impact of these transport differences on the hemispheric water vapor asymmetry, with a moister NH than SH, is not evident from this analysis and will be analyzed in a following paper.

5.3. Horizontal Transport Versus Midlatitude Convection

[67] Recently, *Anderson et al.* [2012] argued for convection at midlatitudes affecting lower stratosphere water vapor up to about 80 hPa, causing a significant impact on ozone chemistry and UV dosage levels. Also, other in situ observations showed enhanced water vapor mixing ratios at midlatitudes related to direct convective injection [e.g., *Hanisco et al.*, 2007; *Dessler and Sherwood*, 2004]. In a very recent paper, *Schwartz et al.* [2013] showed evidence that also MLS observes enhanced water vapor mixing ratios at 100/82 hPa (up to 18/12 ppmv) during summer, particularly above North America and Asia, albeit these observations occur very rarely in the 8 year MLS record.

[68] Our model simulation shows water vapor mixing ratios in NH midlatitudes (370–420 K) up to about 12 ppmv (see water vapor pdf in Figure 10a), in good agreement with MLS observations, and without explicitly including convection in the model. These high mixing ratios completely disappear in the model simulation with a transport barrier at 35°N, blocking all horizontal transport between low and midlatitudes. A transport barrier at 15°N shows an almost vanishing effect. Therefore, our model simulations show clear evidence for the high water vapor mixing ratios in NH midlatitudes linked to horizontal transport from the subtropics. Transport related to subtropical convection within the monsoons and subsequent horizontal intrusions into midlatitudes occurs on timescales of about a week. Therefore, distinguishing this transport from direct convective injection at midlatitudes represents a difficult task, regarding the interpretation of water vapor measurements.

[69] A noteworthy difference compared to, e.g., *Anderson et al.* [2012] and *Schwartz et al.* [2013] is the restriction of our analysis to equivalent latitudes poleward 40°N to separate midlatitude from (sub-)tropical air. A recent study by Kunz et al. (Extending water vapor trend observations over Boulder into the tropopause region: Trend uncertainties and resulting radiative forcing, submitted to *Journal of Geophysical Research*, 2013) showed that separating midlatitude from tropical air masses is a challenging task when analyzing water vapor close to the subtropical jet. Using this equivalent latitude criterion, the highest mixing ratios found in MLS observations and in the model are about 12 ppmv. Without an equivalent latitude restriction, we find a much more pronounced tail of the water vapor mixing ratio pdf (Figure 10b), and highest mixing ratios up to 18 ppmv, as high as have been observed by *Anderson et al.* [2012] and *Schwartz et al.* [2013]. This analysis suggests that the high-reaching convection, which causes the enhanced water vapor mixing ratios, occurs largely in the (sub-)tropics, mainly in the Asian and North American monsoons. The subtropical large-scale monsoon convection is included in the model as far as it is included in the large-scale ECMWF wind and heating rate fields. Subsequently, the moist air masses are transported isentropically poleward to midlatitudes and high latitudes. In summary, our model results cannot prove that there is no deep convection at midlatitudes moistening the lower stratosphere. But our results indicate that the impact of such processes on the mean midlatitude water vapor budget is very small.

5.4. Asian Versus American Monsoon Impact

[70] Within the CLaMS model simulation, high water vapor mixing ratios in the NH lower stratosphere are strongly correlated with large fractions of air originating in the Asian and American monsoons (see Figure 14). However, in NH midlatitudes, the fraction of Asian monsoon air may exceed 25% and is about 1 order of magnitude larger than the fraction of American monsoon air. Hence, in order for both monsoons to have a similar impact on NH water vapor, the mean mixing ratio in the American monsoon would have to be about 1 order of magnitude higher than in the Asian monsoon. Figure 4 shows that this is not the case and that water vapor mixing ratios inside both monsoons are very similar. However, due to the strong dependence of simulated water vapor on the reliability of reanalysis temperatures, as well as on ice microphysics and convection, we cannot reliably state whether the highest mixing ratios observed in the NH lower stratosphere originate within the American or the Asian monsoon.

[71] A caveat to our analysis may result from the moister American monsoon region in MLS observations compared to the model simulation. Recent papers [e.g., *Randel et al.*, 2012; *Schwartz et al.*, 2013] show an impact of deep convection in the monsoon regions on UTLS composition. Consequently, the difference between model and observations could indicate missing convection in the model but could also be related to temperature (and tropopause height) biases in ECMWF data, a fact which needs further study.

[72] However, our model simulation shows a strong influence of the Asian monsoon on the composition of air in the NH lower stratosphere, extending from NH summer to fall. The same upward transport within the Asian monsoon and subsequent horizontal transport to high latitudes has recently been proposed to be important also for sulfur-containing species from volcanic eruptions [*Bourassa et al.*, 2012].

5.5. Critical Remarks

[73] Temperature biases in the tropics and subtropics may affect the water vapor simulation at extratropical latitudes. Therefore, the simulated water vapor values should not be overstated, and we emphasize the seasonal and regional patterns of water vapor transport here. In particular, the good agreement between the model simulated and MLS observed water vapor variability (e.g., in Figure 6) indicates a reliable horizontal transport in ERA-Interim, even representing realistic small-scale structures.

[74] Water vapor mixing ratios from the Lagrangian CLaMS model simulation agree well with MLS observations, although pure backtrajectory studies predict a dry bias arguing for a cold bias of ERA-Interim tropical tropopause temperatures [e.g., *Liu et al.*, 2011; *Schoeberl et al.*, 2012]. However, the ERA-Interim cold bias, particularly around 100 hPa until the end of 2006, appears too small to explain the entire dry bias [*Fueglistaler et al.*, 2013]. Three effects in the CLaMS model cause an additional moistening compared to pure trajectory calculations. First, including a physically based finite terminal settling velocity in the dehydration scheme has a globally, almost uniform, moistening effect of about 0.5 ppmv compared to a sensitivity simulation with instantaneous fall-out of ice and therefore is comparable to an effective temperature correction for the low bias of ERA-Interim tropopause temperatures. Because the effects of a finite settling time on stratospheric water vapor in the model are very similar to the effects of supersaturation, our results are no hint that supersaturation effects are unimportant. It should be noted that the computation of the terminal settling velocity is based on local temperature and ice particle radius. Second, irreversible small-scale mixing, as parameterized in the CLaMS model, causes moistening of the lower stratosphere due to diffusive water vapor transport across the tropopause [*Riese et al.*, 2012]. Water vapor mixing ratios from a purely advective CLaMS sensitivity simulation without any irreversible small-scale mixing are substantially dryer (e.g., about 0.5 ppmv at 390 K), compared to the simulation discussed here. Furthermore, restricting backtrajectory ensembles to only troposphere-to-stratosphere transport trajectories, as is done in many pure trajectory analyses, excludes a moistening effect of transport from the extratropical lower stratosphere on tropical entry water vapor mixing ratios.

5.6. Final Conclusions

[75] The impact of subtropical processes, like transport by monsoons and subtropical jets, and subsequent horizontal transport on water vapor in the NH lower stratosphere raises the question about changes of these processes in a changing climate. In addition to the direct effect of temperature changes on water vapor via freeze-drying, the effects of changing temperatures on wave breaking and related changes in horizontal transport (residual circulation and eddy mixing) seem to be of critical importance. In particular, providing global observations and simulations at high spatial and temporal resolution represents a crucial task for understanding these complex interactions.

[76] **Acknowledgments.** We thank N. Thomas for programming support, W. Read, L. Hoffmann and M. Abalos for helpful discussions, and the ECMWF for providing reanalysis data.

References

Abalos, M., W. J. Randel, and E. Serrano (2012), Variability in upwelling across the tropical tropopause and correlations with tracers in the lower stratosphere, *Atmos. Chem. Phys.*, *12*, 11,505–11,517.

Anderson, J. G., D. M. Wilmouth, J. B. Smith, and D. S. Sayres (2012), UV dosage levels in summer: Increased risk of ozone loss from convectively injected water vapor, *Science*, *17*, 835–839.

Andrews, D. G., J. R. Holton, and C. B. Leovy (1987), *Middle Atmosphere Dynamics*, Academic Press, San Diego, USA.

Bannister, R. N., A. ONeill, A. R. Gregory, and K. M. Nissen (2004), The role of the south-east Asian monsoon and other seasonal features in creating the "tape-recorder" signal in the Unified Model, *Q. J. R. Meteorol. Soc.*, *130*, 1531–1554.

Berthet, G., J. G. Esler, and P. H. Haynes (2007), A Lagrangian perspective of the tropopause and the ventilation of the lowermost stratosphere, *J. Geophys. Res.*, *112*, D18102, doi:10.1029/2006JD008295.

Bian, J., L. L. Pan, L. Paulik, H. Vömel, H. Chen, and D. Lu (2012), In situ water vapor and ozone measurements in Lhasa and Kunming during the Asian summer monsoon, *Geophys. Res. Lett.*, *39*, L19808, doi:10.1029/2012GL052996.

Birner, T. (2006), Fine-scale structure of the extratropical tropopause region, *J. Geophys. Res.*, *111*, D04104, doi:10.1029/2005JD006301.

Birner, T., and H. Bönisch (2011), Residual circulation trajectories and transit times into the extratropical lowermost stratosphere, *Atmos. Chem. Phys.*, *11*, 817–827.

Birner, T., A. Dörnbrack, and U. Schumann (2002), How sharp is the tropopause at midlatitudes? *Geophys. Res. Lett.*, *29*(14), 1700, doi:10.1029/2002GL015142.

Bönisch, H., A. Engel, J. Curtius, T. Birner, and P. Hoor (2008), Quantifying transport into the lowermost stratosphere using simultaneous in-situ measurements of SF_6 and CO_2, *Atmos. Chem. Phys.*, *10*, 5905–5919.

Bönisch, H., A. Engel, T. Birner, P. Hoor, D. W. Tarasick, and E. A. Ray (2011), On the structural changes in the Brewer-Dobson circulation after 2000, *Atmos. Chem. Phys.*, *11*, 3937–3948.

Bourassa, A. E., A. Robock, W. J. Randel, T. Deshler, L. A. Rieger, N. D. Lloyd, E. J. Llewellyn, and D. A. Degenstein (2012), Large volcanic aerosol load in the stratosphere linked to Asian monsoon transport, *Science*, *337*(78), 78–81.

Dessler, A. E., and S. C. Sherwood (2004), Effect of convection on the summertime extratropical lower stratosphere, *J. Geophys. Res.*, *109*, D23301, doi:10.1029/2004JD005209.

Dethof, A., A. O'Neill, J. M. Slingo, and H. G. J. Smit (1999), A mechanism for moistening the lower stratosphere involving the Asian summer monsoon, *Q. J. R. Meteorol. Soc.*, *125*, 1079–1106.

Fischer, H., F. G. Wienhold, P. Hoor, O. Bujok, C. Schiller, P. Siegmund, M. Ambaum, H. A. Scheeren, and J. Lelieveld (2000), Tracer correlations in the northern high latitude lowermost stratosphere: Influence of cross-tropopause mass exchange, *Geophys. Res. Lett.*, *27*(1), 97–100.

Forster, P., and K. P. Shine (1999), Stratospheric water vapour change as possible contributor to observed stratospheric cooling, *Geophys. Res. Lett.*, *26*(21), 3309–3312.

Fueglistaler, S., M. Bonazzola, P. H. Haynes, and T. Peter (2005), Stratospheric water vapor predicted from the Lagrangian temperature history of air entering the stratosphere in the tropics, *J. Geophys. Res.*, *110*(D8), D08107, doi:10.1029/2004JD005516.

Fueglistaler, S., A. E. Dessler, T. J. Dunkerton, I. Folkins, Q. Fu, and P. W. Mote (2009a), Tropical tropopause layer, *Rev. Geophys.*, *47*, RG1004, doi:10.1029/2008RG000267.

Fueglistaler, S., B. Legras, A. Beljaars, J. J. Morcrette, A. Simmons, A. M. Tompkins, and S. Uppala (2009b), The diabatic heat budget of the upper troposphere and lower/mid stratosphere in ECMWF reanalysis, *Q. J. R. Meteorol. Soc.*, *135*, 638.

Fueglistaler, S., et al. (2013), The relation between atmospheric humidity and temperature trends for stratospheric water, *J. Geophys. Res. Atmos.*, *118*, 1052–1074, doi:10.1002/jgrd.50157.

Gettelman, A., D. E. Kinnison, and T. J. Dunkerton (2004), Impact of monsoon circulations on the upper troposphere and lower stratosphere, *J. Geophys. Res.*, *109*, D22101, doi:10.1029/2004JD004878.

Gettelman, A., P. Hoor, L. L. Pan, W. J. Randel, M. I. Hegglin, and T. Birner (2011), The extratropical upper troposphere and lower stratosphere, *Rev. Geophys.*, *49*, RG3003, doi:10.1029/2011RG000355.

Günther, G., R. Müller, M. von Hobe, F. Stroh, P. Konopka, and C. M. Volk (2008), Quantification of transport across the boundary of the lower stratospheric vortex during Arctic winter 2002/2003, *Atmos. Chem. Phys.*, *8*(13), 3655–3670.

Hanisco, T. F., et al. (2007), Observations of deep convective influence on stratospheric water vapor and its isotopic composition, *Geophys. Res. Lett.*, *34*, L04814, doi:10.1029/2006GL027899.

Haynes, P., and E. Shuckburgh (2000), Effective diffusivity as a diagnostic of atmospheric transport 2. Troposphere and lower stratosphere, *J. Geophys. Res.*, *105*(D18), 22,795–22,810.

Hegglin, M. I., and T. G. Shepherd (2007), O_3-N_2O correlations from the Atmospheric Chemistry Experiment: Revisiting a diagnostic of transport and chemistry in the stratosphere, *J. Geophys. Res.*, *112*, D19301, doi:10.1029/2006JD008281.

Hegglin, M. I., C. D. Boone, G. L. Manney, and K. A. Walker (2009), A global view of the extratropical tropopause transition layer from atmospheric chemistry experiment Fourier transform spectrometer O_3, H_2O, and CO, *J. Geophys. Res.*, *114*, D00B11, doi:10.1029/2008JD009984.

Holton, J. R., P. Haynes, M. E. McIntyre, A. R. Douglass, R. B. Rood, and L. Pfister (1995), Stratosphere-troposphere exchange, *Rev. Geophys.*, *33*, 403–439.

Homeyer, C. R., and K. P. Bowman (2012), Rossby wave breaking and transport between the tropics and extratropics above the subtropical jet, *J. Atmos. Sci.*, *70*, 607–626.

Hoor, P., H. Fischer, L. Lange, J. Lelieveld, and D. Brunner (2002), Seasonal variations of a mixing layer in the lowermost stratosphere as identified by the CO-O_3 correlation from in situ measurements, *J. Geophys. Res.*, *107*(D5), 4044, doi:10.1029/2000JD000289.

Hoor, P., C. Gurk, D. Brunner, M. I. Hegglin, H. Wernli, and H. Fischer (2004), Seasonality and extent of extratropical TST derived from in-situ CO measurements during SPURT, *Atmos. Chem. Phys.*, *4*, 1427–1442.

James, R., M. Bonazzola, B. Legras, K. Surbled, and S. Fueglistaler (2008), Water vapor transport and dehydration above convective outflow during Asian monsoon, *Geophys. Res. Lett.*, *35*, L20810, doi:10.1029/2008GL035441.

Jensen, E. J., and L. Pfister (2004), Transport and freeze-drying in the tropical tropopause layer, *J. Geophys. Res.*, *109*, D02207, doi:10.1029/2003JD004022.

Jones, R. L., and J. A. Pyle (1984), Observations of CH_4 and N_2O by the NIMBUS 7 SAMS: A comparison with in situ data and two-dimensional numerical model calculations, *J. Geophys. Res.*, *89*, 5263–5279.

Konopka, P., J.-U. Grooß, F. Ploeger, and R. Müller (2009), Annual cycle of horizontal in-mixing into the lower tropical stratosphere, *J. Geophys. Res.*, *114*, D19111, doi:10.1029/2009JD011955.

Konopka, P., et al. (2004), Mixing and ozone loss in the 1999-2000 Arctic vortex: Simulations with the 3-dimensional Chemical Lagrangian Model of the Stratosphere (CLaMS), *J. Geophys. Res.*, *109*, D02315, doi:10.1029/2003JD003792.

Konopka, P., et al. (2007), Contribution of mixing to upward transport across the tropical tropopause layer (TTL), *Atmos. Chem. Phys.*, *7*, 3285–3308.

Krämer, M., et al. (2009), Ice supersaturations and cirrus cloud crystal numbers, *Atmos. Chem. Phys.*, *9*, 3505–3522.

Kunz, A., P. Konopka, R. Müller, L. L. Pan, C. Schiller, and F. Rohrer (2009), High static stability in the mixing layer above the extratropical tropopause, *J. Geophys. Res.*, *114*, D16305, doi:10.1029/2009JD011840.

Kunz, A., P. Konopka, R. Müller, and L. L. Pan (2011), Dynamical tropopause based on isentropic potential vorticity gradients, *J. Geophys. Res.*, *116*, D01110, doi:10.1029/2010JD014343.

Lambert, A., et al. (2007), Validation of the Aura Microwave Limb Sounder middle atmosphere water vapor and nitrous oxide measurements, *J. Geophys. Res.*, *112*, D24S36, doi:10.1029/2007JD008724.

Liu, S., S. Fueglistaler, and P. Haynes (2011), Advection-condensation paradigm for stratospheric water vapor, *J. Geophys. Res.*, *115*, D24307, doi:10.1029/2010JD014352.

Livesey, N. J., et al. (2011), Earth Observing System (EOS) Aura Microwave Limb Sounder MLS version 3.3 level 2 data quality and description document, *http://mls.jpl.nasa.gov/data/v3-3_data_quality_document.pdf*.

Mahowald, N. M., R. A. Plumb, P. J. Rasch, J. del Corral, and F. Sassi (2002), Stratospheric transport in a three-dimensional isentropic coordinate model, *J. Geophys. Res.*, *107*(D15), 4254, doi:10.1029/2001JD001313.

McIntyre, M. E., and T. N. Palmer (1983), Breaking planetary waves in the stratosphere, *Nature*, *305*, 593–600.

McKenna, D. S., J.-U. Grooß, G. Günther, P. Konopka, R. Müller, G. Carver, and Y. Sasano (2002a), A new chemical lagrangian model of the stratosphere (CLaMS): 2. Formulation of chemistry scheme and initialization, *J. Geophys. Res.*, *107*(D15), 4256, doi:10.1029/2000JD000113.

McKenna, D. S., P. Konopka, J.-U. Grooß, G. Günther, R. Müller, R. Spang, D. Offermann, and Y. Orsolini (2002b), A new Chemical Lagrangian Model of the Stratosphere (CLaMS): 1. Formulation of advection and mixing, *J. Geophys. Res.*, *107*(D16), 4309, doi:10.1029/2000JD000114.

Mote, P. W., K. H. Rosenlof, M. E. McIntyre, E. S. Carr, J. C. Gille, J. R. Holton, J. S. Kinnersley, H. C. Pumphrey, J. M. Russell III, and J. W . Waters (1996), An atmospheric tape recorder: The imprint of tropical tropopause temperatures on stratospheric water vapor, *J. Geophys. Res.*, *101*(D2), 3989–4006.

Nash, E. R., P. A. Newman, J. E. Rosenfield, and M. R. Schoeberl (1996), An objective determination of the polar vortex using Ertel's potential vorticity, *J. Geophys. Res.*, *101*, 9471–9478.

Olsen, M. A., A. R. Douglas, M. R. Schoeberl, J. M. Rodriquez, and Y. Yoshida (2010), Interannual variability of ozone in the winter lower stratosphere and the relationship to lamina and irreversible transport, *J. Geophys. Res.*, *115*, D15305, doi:10.1029/2009JD013004.

Pan, L. L., S. Solomon, W. Randel, J.-F. Lamarque, P. Hess, J. Gille, E.-W. Chiou, and M. P. McCormick (1997), Hemispheric asymmetries and seasonal variations of the lowermost stratospheric water vapor and ozone derived from SAGE II data, *J. Geophys. Res.*, *102*(D23), 28,177–28,184.

Pan, L. L., W. J. Randel, J. C. Gille, B. N. W. D. Hall, S. Massie, V. Yudin, R. Khosravi, P. Konopka, and D. Tarasick (2009), Tropospheric intrusions associated with the secondary tropopause, *J. Geophys. Res.*, *114*, D10302, doi:10.1029/2008JD011374.

Park, M., W. J. Randel, A. Gettelman, S. T. Massie, and J. H. Jiang (2006), Transport above the Asian summer monsoon anticyclone inferred from aura microwave limb sounder tracers, *J. Geophys. Res.*, *112*, D16309, doi:10.1029/2006JD008294.

Ploeger, F., P. Konopka, G. Günther, J.-U. Grooß, and R. Müller (2010), Impact of the vertical velocity scheme on modeling transport in the tropical tropopause layer, *J. Geophys. Res.*, *115*, D03301, doi:10.1029/2009JD012023.

Ploeger, F., et al. (2011), Insight from ozone and water vapour on transport in the tropical tropopause layer (TTL), *Atmos. Chem. Phys.*, *11*, 407–419.

Ploeger, F., F. Ploeger, P. Konopka, R. Müller, S. Fueglistaler, T. Schmidt, J. Manners, J.-U. Grooss, G. Günther, P. M. de Forster, and M. Riese (2012), Horizontal transport affecting trace gas seasonality in

the tropical tropopause layer TTL, *J. Geophys. Res.*, *117*, D09303, doi:10.1029/2011JD017267.

Plumb, R. A. (2002), Stratospheric transport, *J. Meteorol. Soc. Jpn.*, *80*(4B), 793–809.

Pommrich, R., R. Müller, J.-U. Grooß, P. Konopka, G. Günther, H.-C. Pumphrey, S. Viciani, F. D'Amato, and M. Riese (2011), Carbon monoxide as a tracer for tropical troposphere-to-stratosphere transport in the chemical lagrangian model of the stratosphere (CLaMS), *Geosci. Model Dev. Discuss.*, *4*, 1185–1211.

Postel, G. A., and M. H. Hitchman (1999), A climatology of Rossby wave breaking along the subtropical tropopause, *J. Atmos. Sci.*, *56*, 359–373.

Randel, W. J., J. C. Gille, A. E. Roche, J. B. Kumer, J. L. Mergenthaler, J. W. Waters, E. F. Fishbein, and W. A. Lahoz (1993), Stratospheric transport from the tropics to middle latitudes by planetary-wave mixing, *Nature*, *365*, 533–535.

Randel, W. J., F. Wu, A. Gettelman, J. Russell, J. Zawodny, and S. Oltmans (2001), Seasonal variation of water vapor in the lower stratosphere observed in halogen occultation experiment data, *J. Geophys. Res.*, *106*(D13), 14,313–14,32.

Randel, W. J., F. Wu, and P. Forster (2007), The extratropical tropopause inversion layer: Global observations with GPS data, and a radiative forcing mechanism, *J. Atmos. Sci.*, *64*, 4489–4496.

Randel, W. J., M. Park, L. Emmons, D. Kinnison, P. Bernath, K. A. Walker, C. Boone, and H. Pumphrey (2010), Asian monsoon transport of pollution to the stratosphere, *Science*, *328*(5978), 611–613.

Randel, W. J., L. Moyer, M. Park, E. Jensen, P. Bernath, K. A. Walker, and C. Boone (2012), Global variations of HDO and HDO/H_2O ratios in the upper troposphere and lower stratosphere derived from ACE–FTS satellite measurements, *J. Geophys. Res.*, *117*, D06303, doi:10.1029/2011JD016632.

Ray, E. A., F. L. Moore, J. W. Elkins, G. S. Dutton, D. W. Fahey, H. Vömel, S. Oltmans, and K. H. Rosenlof (1999), Transport into the northern hemisphere lowermost stratosphere revealed by in situ tracer measurements, *J. Geophys. Res.*, *104*, 26,565–26,580.

Ray, E. A., et al. (2010), Evidence for changes in stratospheric transport and mixing over the past three decades based on multiple data sets and tropical leaky pipe analysis, *J. Geophys. Res.*, *115*, D21304, doi:10.1029/2010JD014206.

Read, W. G., et al. (2007), Aura Microwave Limb Sounder upper tropospheric and lower stratospheric H_2O and relative humidity with respect to ice validation, *J. Geophys. Res.*, *112*, D24S35, doi:10.1029/2007JD008752.

Riese, M., G. L. Manney, J. Oberheide, X. Tie, R. Spang, and V. Küll (2002), Stratospheric transport by planetary wave mixing as observed during CRISTA-2, *J. Geophys. Res.*, *107*(D23), 8179, doi:10.1029/2001JD000629.

Riese, M., F. Friedl-Vallon, R. Spang, P. Preusse, C. Schiller, L. Hoffmann, H. Oelhaf, T. von Clarmann, and M. Höpfner (2005), Global Limb Radiance Imager for the Atmosphere (GLORIA): Scientific objectives, *Adv. Space Res.*, *36*, 989–995.

Riese, M., F. Ploeger, A. Rap, B. Vogel, P. Konopka, M. Dameris, and P. M. Forster (2012), Impact of uncertainties in atmospheric mixing on simulated UTLS composition and related radiative effects, *J. Geophys. Res.*, *117*, D16305, doi:10.1029/2012JD017751.

Rohs, S., C. Schiller, M. Riese, A. Engel, U. Schmidt, T. Wetter, I. Levin, T. Nakazawa, and S. Aoki (2006), Long-term changes of methane and hydrogen in the stratosphere in the period 1978–2003 and their impact on the abundance of stratospheric water vapor, *J. Geophys. Res.*, *111*, D14315, doi:10.1029/2005JD006877.

Rosenlof, K. H., A. F. Tuck, K. K. Kelly, J. M. Russell III, and M. P. McCormick (1997), Hemispheric asymmetries in the water vapor and inferences about transport in the lower stratosphere, *J. Geophys. Res.*, *102*, 13,213–13,234.

Schiller, C., J.-U. Grooß, P. Konopka, F. Ploeger, F. H. S. dos Santos, and N. Spelten (2009), Hydration and dehydration at the tropical tropopause, *Atmos. Chem. Phys.*, *9*, 9647–9660.

Schoeberl, M. R., and A. E. Dessler (2011), Dehydration of the stratosphere, *Atmos. Chem. Phys.*, *11*, 8433–8446.

Schoeberl, M. R., A. E. Dessler, and T. Wang (2012), Simulation of stratospheric water vapor and trends using three reanalyses, *Atmos. Chem. Phys.*, *12*, 6475–6487.

Schwartz, M. J., W. G. Read, M. L. Santee, N. J. Livesey, L. Froidevaux, A. Lambert, and G. L. Manney (2013), Convectively injected water vapor in the North American summer lowermost stratosphere, *Geophys. Res. Lett.*, *40*, 1–6, doi:10.1002/grl.50421.

Solomon, S., K. H. Rosenlof, R. W. Portmann, J. Daniel, S. M. Davis, T. J. Sanford, and G. K. Plattner (2010), Contributions of stratospheric water vapor to decadal changes in the rate of global warming, *Science*, *327*, 1219–1223.

von Hobe, M., J.-U. Grooß, G. Günther, et al. (2011), Evidence for heterogeneous chlorine activation in the tropical UTLS, *Atmos. Chem. Phys.*, *11*, 241–256.

Waugh, D. W. (1996), Seasonal variation of isentropic transport out of the tropical stratosphere, *J. Geophys. Res.*, *101*, 4007–4023.

World Meteorological Organization (1957), Meteorology–A three-dimensional science, *WMO Bull*, pp. 134–138.

Wright, J. S., R. Fu, S. Fueglistaler, Y. S. Liu, and Y. Zhang (2011), The influence of summertime convection over Southeast Asia on water vapor in the tropical stratosphere, *J. Geophys. Res.*, *116*, D12302, doi:10.1029/2010JD015416.